

# Determination of CKM matrix element and axial vector form factors from weak decays of quantum-entangled strange baryons

The BESIII Collaboration<sup>†</sup>

## Abstract

The electromagnetic structure of the nucleon, parameterized by values such as its charge radius and magnetic moment, can be determined from the scattering of electrons off a nucleon target [1, 2]. However, to study its axial structure, neutrino beams are required [3]. The results from these experiments should be extrapolated to zero energy-momentum transfers to access the static properties of the nucleon [4]. For baryons with strange quarks, hyperons, the static limit can instead be approached in semi-leptonic decays, which give direct access to the weak magnetism and axial-vector coupling strengths that are inaccessible in electromagnetic interactions. The axial-vector coupling describes how the spin structure is transferred from the initial hyperon to the final baryon, while weak magnetism coupling reflects how the baryon's electromagnetic properties are affected by the weak interaction. Both these couplings and the overall normalization, given by form factor  $f_1^*$ , are being determined with increased precision from the theory of strong interactions using a first principles formulation on the space-time lattice [5]. Furthermore, the probability of the semi-leptonic hyperon decay is approximately proportional to  $|V_{us}|^2 \cdot (f_1^2 + 3g_1^2)$ , where  $V_{us}$  is the matrix element of the Cabibbo–Kobayashi–Maskawa (CKM) matrix responsible for the transition between an  $s$  and a  $u$  quark. Current determinations of  $|V_{us}|$  come from kaon decays [6], but the results are not consistent and could indicate a deviation from CKM matrix unitarity, a tell-tale sign of physics beyond the Standard Model (SM) of elementary particles. Here we determine the absolute branching fraction and weak coupling strengths,  $g_{av} \equiv g_1/f_1$ , for  $\Lambda \rightarrow pe^-\bar{\nu}_e$ ,  $g_{av} = 0.742^{+0.075}_{-0.057} \pm 0.009$ , and  $\bar{\Lambda} \rightarrow \bar{p}e^+\nu_e$ ,  $g_{av}^+ = -0.706^{+0.069}_{-0.073} \pm 0.014$ . These observables combined with form factors determined from first-principle lattice QCD calculations allow for the extraction of the  $|V_{us}|$  value. The first measurement of the  $\Lambda$  weak electricity coupling, i.e.  $g_{av2} \equiv g_2/f_1 = -0.189^{+0.651}_{-0.629}$ , is consistent with flavour SU(3) symmetry conservation. We demonstrate how  $|V_{us}|$  can be extracted with increasing sensitivity using polarized hyperons from entangled, baryon-antibaryon pairs, thus enabling a complementary road to that of meson decays. In addition, the presented experimental method can be used, *mutatis mutandis*, for other semileptonic decays of baryons.

<sup>†</sup>A full list of authors and affiliations appears in the online version of this paper.

<sup>\*</sup>Throughout this Letter,  $f_i \equiv f_i(0)$  and  $g_i \equiv g_i(0)$  are implied unless explicitly noted.

Transition form factors are fundamental hadron properties describing the dynamic behaviour of the transition between two states. The transition matrix element for a semi-leptonic weak decay of a hyperon is parameterized by six form factors,  $f_i(q^2)$  and  $g_i(q^2)$  ( $i = 1, 2, 3$ ). These represent the vector and axial vector parts of the weak interaction, respectively, and depend on the squared momentum transfer,  $q^2$ , of the intermediate  $W$  boson. Since both the induced scalar ( $f_3$ ) and pseudoscalar ( $g_3$ ) form factors are suppressed by the squared ratio of the lepton to hyperon mass, the electron–antineutrino decay modes effectively depend only on four form factors and  $V_{us}$ , as depicted in Figure 1.

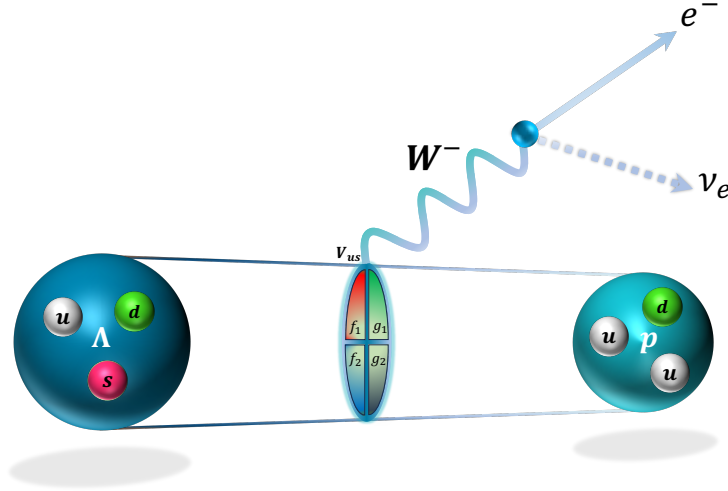


Fig. 1 Schematic representation of the  $\Lambda$  decay to a proton, an electron and an electric anti-neutrino via virtual (mediating)  $W^-$  boson.

When neglecting the  $q^2$  dependence of the form factors, the branching ratio  $\mathcal{B}$  of the semi-leptonic decay  $\Lambda \rightarrow p e^- \bar{\nu}_e$  is given by [7]:

$$\mathcal{B} = \frac{\tau_\Lambda}{\hbar} G_F^2 |V_{us}|^2 \frac{\beta^5 M_\Lambda^5}{60\pi^3} \left[ \left(1 - \frac{3}{2}\beta\right)(f_1^2 + 3g_1^2) - 4\beta g_1 g_2 + \frac{2}{7}\beta^2 \mathcal{F}_2 + O(\beta^3) \right], \quad (1)$$

where  $\beta = (M_\Lambda - M_p)/M_\Lambda$ , with  $M_\Lambda$  and  $M_p$  denoting the masses of the  $\Lambda$  and proton, respectively. The weak decay constant  $G_F$  and the  $\Lambda$  lifetime  $\tau_\Lambda$  are known with high accuracy [8]. The form factor dependent function  $\mathcal{F}_2$  is defined in Methods. The ratios  $g_1/f_1$ ,  $f_2/f_1$  and  $g_2/f_1$  represent the axial vector ( $g_{av} \equiv g_1/f_1$ ), weak magnetism ( $g_w \equiv f_2/f_1$ ), and weak electricity ( $g_{av2} \equiv g_2/f_1$ ) couplings at zero momentum transfer  $q^2$ , respectively. Therefore, the precise measurement of the decay branching fraction can be used to determine  $|V_{us}|$  if the form factors are known. The relative couplings,  $g_{av}$ ,  $g_w$  and  $g_{av2}$ , can be determined from angular distributions, but a reliable theoretical determination of  $f_1$  depends on the ability to describe the subtle differences between the  $d$ - and  $s$ -quarks [9]. Here, approximate flavour SU(3) symmetry serves as a good approximation confirmed by previous experimental results [10–12]. For instance,  $f_1$  is protected from leading-order SU(3)-breaking effects. However, corrections

are essential at next-to-leading order [13]. There are various model estimates of  $f_1$  using quark models [14, 15], large- $N_c$  [16–19] and chiral expansions [20–22], and QCD sum rules [23]. A drawback is that these models disagree on the size of the SU(3)-breaking corrections, which affects the precision of  $|V_{us}|$  [24]. In the last decade, lattice QCD joined the effort to predict  $f_1$  using a non-perturbative method [25–27] and a model-independent approach [28] developed for the form factors of meson decays [29, 30]. Still, understanding the quark mass dependence of SU(3)-breaking remains a crucial issue.

Another way to determine the vector form factor is indirectly via the  $g_{av}$  coupling and  $g_1$  form factor. The  $g_{av}$  coupling has been measured experimentally [10–12], with the most precise determination performed more than thirty years ago by a Fermilab-based fix-target experiment using a neutral-hyperon beam [12], which observed  $\sim 37 \cdot 10^3$   $\Lambda \rightarrow pe^- \bar{\nu}_e$  candidates. The average value based on the Particle Data Group gives  $g_{av} = 0.718 \pm 0.015$  [8]. In contrast to  $f_1$ , the axial vector form factor is not protected by the Ademollo-Gatto theorem [13]. Thus, SU(3)-breaking corrections must be already considered at leading order. During the last several years the  $g_1$  of hyperon beta decays have been calculated with high accuracy from first principles using the techniques of lattice QCD [31]. As the hyperon axial form factor can be determined from the lattice, and since there is currently not enough experimental information, its value serves as an important cross-validation, especially crucial for physics related to neutrino experiments, which often must rely on theoretical modeling [32]. The weak electricity coupling,  $g_{av2}$ , is intimately linked to SU(3) symmetry. In the absence of second-class currents, it vanishes in the SU(3) limit [9]. This quantity has so far only been determined once for a weakly decaying baryon. This was performed by the KTeV experiment for the process  $\Xi^0 \rightarrow \Sigma^+ e^- \bar{\nu}_e$  decay [33] and was found to be consistent with zero.

The CKM matrix element  $|V_{us}|$  was evaluated by Cabibbo using  $\Lambda$  semi-leptonic decay [9, 34]. The analyses were based on the determination of relative branching fractions [10] and the  $g_{av}$  coupling [12] while the values of  $f_2$  and  $g_2$  were predicted within the conserved vector current (CVC) hypothesis [35] and SU(3) symmetry limit [9, 34], respectively. The obtained precision was found to be  $\sigma(|V_{us}|) \sim 0.0034$  while precise experimental measurements are required in order to be competitive with the precision from kaon decays,  $\sigma(|V_{us}|) \sim 0.0009$  [8]. Thus, in comparison to the traditional way of determining  $|V_{us}|$  using kaon decays, where the accuracy is limited by knowledge of decay constants in lattice QCD calculation [36], more studies are required for the relevant hadronic matrix elements to reach the same level [36].

In this article, we determine the absolute branching fraction for  $\Lambda \rightarrow pe^- \bar{\nu}_e$  and the couplings  $g_{av}$ ,  $g_w$  and  $g_{av2}$  simultaneously. We provide two values of  $|V_{us}|$ , one under the assumption of SU(3) symmetry conservation, and the other using the lattice QCD determination of the form factors. Additionally the product of  $|V_{us}|$  and the dominant form factor combination,  $|V_{us}| \cdot \sqrt{f_1^2 + 3g_1^2}$ , has been extracted for the first time for any semi-leptonic baryon decay.

The method, developed in Refs. [37, 38], uses entangled baryon–antibaryon pairs with polarization in the process  $e^+e^- \rightarrow J/\psi \rightarrow \Lambda(\rightarrow pe^- \bar{\nu}_e)\bar{\Lambda}(\rightarrow \bar{p}\pi^+)$  with its corresponding charge-conjugated  $\Lambda\bar{\Lambda}$  decay modes. The production of the  $\Lambda$  pairs with their subsequent decays are described with seven kinematic variables: six helicity angles and the four-momentum transfer between the  $\Lambda$  and proton,  $\xi = \{\theta, \theta_p, \phi_p, \theta_e, \theta_{\bar{p}}, \phi_{\bar{p}}, q^2\}$ . The helicity angles are determined by boosting and rotating the particles into their respective helicity frames (Figure 2). The production process is characterized by the  $\Lambda$  scattering angle relative

to the positron beam axis in the center-of-momentum (c.m.) frame,  $\theta$ . The angles  $\theta_p$  and  $\phi_p$  ( $\theta_{\bar{p}}$  and  $\phi_{\bar{p}}$ ) are defined with respect to the proton (anti-proton) direction in the reference system  $\mathcal{R}_\Lambda$  ( $\mathcal{R}_{\bar{\Lambda}}$ ), where  $\Lambda(\bar{\Lambda})$  is at rest and where the  $\hat{z}$  axis points in the direction of the  $\Lambda(\bar{\Lambda})$  in the c.m. system. The  $\hat{y}$  axis is perpendicular to the production plane. The angle  $\theta_e$  and the four-momentum transfer  $q^2$  gives the direction of the electron (positron) in the direction of the  $\Lambda(\bar{\Lambda})$  in the  $\mathcal{R}_\Lambda$  ( $\mathcal{R}_{\bar{\Lambda}}$ ) frame. The structure of the seven-dimensional angular distribution is determined by six global parameters  $\omega = \{\alpha_\psi, \Delta\Phi, g_{av}, g_w, g_{av2}, \alpha_+(\alpha_-)\}$  and can be expressed in a modular form as [38]:

$$\mathcal{W}(\xi, \omega) = \sum_{\mu, \bar{\nu}=0}^3 C_{\mu\bar{\nu}} R_{\mu\kappa}(\Omega_p) b_{\kappa 0}^\Lambda a_{\bar{\nu} 0}^{\bar{\Lambda}} + c.c. \quad (2)$$

The production term  $C_{\mu\bar{\nu}}(\theta_\Lambda; \alpha_\psi, \Delta\Phi)$  is a  $4 \times 4$  spin density matrix describing the polarization and the spin correlations between the  $\Lambda$  pair and is defined in the reference frames  $\mathcal{R}_\Lambda$  and  $\mathcal{R}_{\bar{\Lambda}}$ . The parameters  $\alpha_\psi$  and  $\Delta\Phi$  are related to two production amplitudes, where  $\alpha_\psi$  governs the  $\Lambda$  angular distribution and  $\sin(\Delta\Phi)$  is proportional to the hyperon polarization [37]. The  $4 \times 4$  matrices  $R_{\mu\kappa} b_{\kappa 0}^\Lambda$  in equation (2) represents the rotation matrix between the  $\Lambda$  and the proton, while  $a_{\bar{\nu} 0}^{\bar{\Lambda}}$  describes the transition from the  $\bar{\Lambda}$  to the anti-proton. The elements of these matrices are parametrized in terms of the helicity angles as well as the weak decay parameters:  $R_{\mu\kappa}(\theta_p, \phi_p) b_{\kappa 0}^\Lambda(\theta_e, q^2; g_{av}, g_w, g_{av2})$  in reference system  $\mathcal{R}_\Lambda$ ,  $a_{\bar{\nu} 0}^{\bar{\Lambda}}(\theta_{\bar{p}}, \phi_{\bar{p}}; \alpha_+)$  in reference system  $\mathcal{R}_{\bar{\Lambda}}$ . The full expressions of  $C_{\mu\bar{\nu}}$ ,  $R_{\mu\kappa} b_{\kappa 0}$  and  $a_{\bar{\nu} 0}$  are given in Refs. [37, 38].

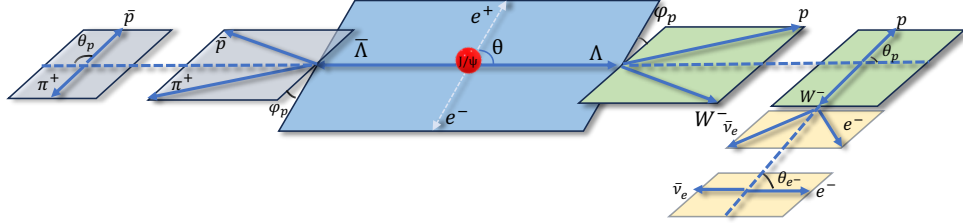


**Fig. 2** Definition of the helicity angles for  $e^+e^- \rightarrow J/\psi \rightarrow \Lambda(\rightarrow p e^- \bar{\nu}_e) \bar{\Lambda}(\rightarrow \bar{p} \pi^+)$ . The angles  $\theta_\Lambda$ ,  $\theta_{\bar{p}}$ ,  $\phi_{\bar{p}}$ ,  $\theta_p$ ,  $\phi_p$ , and  $\theta_e$  are the helicity angles of the  $\Lambda$ ,  $\bar{p}$ ,  $p$ , and lepton in the  $e^+e^-$  c.m. system (blue area),  $\bar{\Lambda}$  rest frame (gray area),  $\Lambda$  rest frame (green area), and  $W^-$  rest frame (yellow area), respectively. In the  $e^+e^-$  c.m. system, the  $\hat{z}$  is along the  $e^+$  momentum direction, and the  $\hat{z}_\Lambda$  ( $\hat{z}_{\bar{\Lambda}}$ ) is along the  $\Lambda$  ( $\bar{\Lambda}$ ) outgoing direction. In the  $\Lambda$  ( $\bar{\Lambda}$ ) rest frame, the polar axis is  $\hat{z}_\Lambda$  ( $\hat{z}_{\bar{\Lambda}}$ ),  $\hat{y}_\Lambda$  ( $\hat{y}_{\bar{\Lambda}}$ ) is along  $\hat{z} \times \hat{z}_\Lambda$  ( $\hat{z} \times \hat{z}_{\bar{\Lambda}}$ ) and  $\hat{z}_W$  is along the  $W^-$  outgoing direction. In the  $W^-$  rest frame, the polar axis is  $\hat{z}_W$ ,  $\hat{y}_W$  is along  $\hat{z}_\Lambda \times \hat{z}_W$ .

Our results are based on the  $(10.087 \pm 0.044) \times 10^9$   $J/\psi$  events collected with the multi-purpose detector BESIII [39]. The  $J/\psi$  resonance decays into a  $\Lambda\bar{\Lambda}$  pair with a probability of  $(1.89 \pm 0.09) \times 10^{-3}$  [8]. All final state particles, except the neutrino, are reconstructed. The particles are electrically charged and can therefore be recorded in the multilayer drift chamber, where a superconducting solenoid provides a magnetic field allowing for momentum determination with an accuracy of 0.5% at 1.0 GeV/c. The semi-leptonic and hadronic  $\Lambda(\bar{\Lambda})$  candidates are identified by combining  $pe^-(\bar{p}e^+)$  pairs and  $\bar{p}\pi^+(p\pi^-)$ , respectively. To obtain electrons/positrons with sufficient quality, their momenta were required to be larger than 0.1 GeV/c<sup>2</sup>. The semi-leptonic decays are identified using the variable  $U_{\text{miss}} =$

$E_{\text{miss}} - c \cdot |\vec{p}_{\text{miss}}|$ , where  $E_{\text{miss}}$  and  $\vec{p}_{\text{miss}}$  denote the missing energy and momentum of the semi-leptonic decay, respectively. For candidates of semi-leptonic decay, the  $U_{\text{miss}}$  distribution is uniformly distributed around zero, while the hadronic  $\Lambda$  background features a right-skewed distribution which peaks at  $U_{\text{miss}} \sim 0.022$  GeV. The signal yield is determined from an extended unbinned maximum likelihood fit [40] of the  $U_{\text{miss}}$  distribution, shown in Figure 3, which combines both  $\Lambda \rightarrow pe^-\bar{\nu}_e$  and  $\bar{\Lambda} \rightarrow \bar{p}e^+\nu_e$ . The signal shape is described using Monte Carlo (MC) simulation convoluted with a Gaussian function to account for the resolution differences between data and MC. The shape of the dominant background contribution,  $\Lambda \rightarrow p\pi^-$ , is obtained using the corresponding MC sample while the rest of the background contribution is described by a linear function. The yields and the parameters of the Gaussian and linear function are floated in the fit. The fit result is integrated over the signal region, defined as  $|U_{\text{miss}}| < 0.02$  GeV, and gives  $1791 \pm 47$  events of  $\Lambda \rightarrow pe^-\bar{\nu}_e + c.c.$  The evaluated background yield in this region is  $207 \pm 30$  events. More details of the selection and analysis procedure are given in Methods.

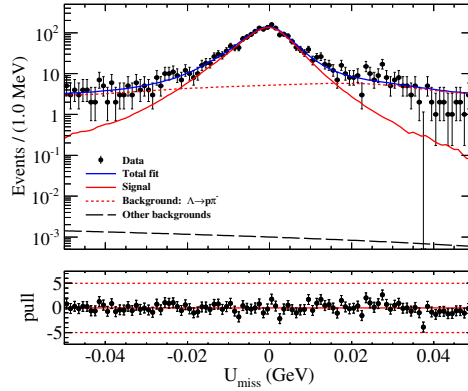


**Fig. 3** The  $U_{\text{miss}}$  distribution of  $\Lambda \rightarrow pe^-\bar{\nu}_e$  and  $\bar{\Lambda} \rightarrow \bar{p}e^+\nu_e$  candidates. The black points with vertical error bars correspond to the number of observed events with statistical uncertainty in each bin. The blue solid line is the total fit which includes the signal yields (red solid), the dominant background contribution (red dotted line) and the other background contributions (black long-dashed line). The pull distribution (bottom panel) shows the agreement between the data and the total fit result.

For the determination of the semi-leptonic absolute branching fraction, we employ the double-tagging (DT) technique, as pioneered in the MARK-III experiment [41]. It has the additional advantage that the four momentum transfer  $q^2$  can be reconstructed unambiguously [42]. We refer to the final event sample where one of the hyperons decays semi-leptonically and its recoiling hyperon partner decays hadronically as the DT sample. The technique also requires knowledge of the so-called single-tag (ST) sample, which provides information about event yield and efficiency when only the two-body hadronic decay of the  $\bar{\Lambda}$  (or  $\Lambda$ ) is reconstructed.

The branching fraction of the semi-leptonic decay of the  $\Lambda$  is determined from

$$\mathcal{B}(\Lambda \rightarrow pe^-\bar{\nu}_e) = \frac{N_{\text{DT}}}{\epsilon_{\text{DT}}} \frac{\epsilon_{\text{ST}}}{N_{\text{ST}}}, \quad (3)$$

where,  $N_{\text{DT}}$  and  $\epsilon_{\text{DT}}$  are the semi-leptonic event yield and detection efficiency in the DT sample, respectively, while  $N_{\text{ST}}$  and  $\epsilon_{\text{ST}}$  are the event yield and detection efficiency obtained using the ST sample. The values of ST yield and detection efficiency for this sample were previously measured to be  $N_{\text{ST}} = (14.328 \pm 0.005) \times 10^6$  and  $\epsilon_{\text{ST}} = (54.09 \pm 0.01)\%$  [43], respectively. The semi-leptonic event yield,  $N_{\text{DT}} = 1854 \pm 49$ , is obtained from the fit as shown in the Fig. 3. The DT detection efficiency,  $\epsilon_{\text{DT}} = (8.58 \pm 0.01)\%$  is determined from a dedicated simulated sample including the production and decay dynamics of the full process. Equation (3) yields  $\mathcal{B}(\Lambda \rightarrow pe^-\bar{\nu}_e) = (8.16 \pm 0.22 \pm 0.15) \times 10^{-4}$  which is in agreement with the world average value of  $\mathcal{B}(\Lambda \rightarrow pe^-\bar{\nu}_e) = (8.34 \pm 0.14) \times 10^{-4}$  [8].

To determine the transition form factors we use the kinematic information in  $\xi$ . This allows us to determine the physical parameters in  $\omega$  by performing an unbinned maximum log-likelihood fit in which the multidimensional reconstruction efficiency is also taken into account. In contrast to previous measurements [10–12] we can exploit the fact that the  $\Lambda$  is produced along with a  $\bar{\Lambda}$  to our advantage. On an event-by-event basis it allows us to fully reconstruct the kinematics of the semi-leptonic decay, while globally, it provides detailed information of the production mechanism of the quantum-entangled  $\Lambda - \bar{\Lambda}$  pair. The  $\Lambda$  polarization and the spin correlations between the pair are uniquely determined by the two production parameters,  $\alpha_\psi$  and  $\Delta\Phi$ . These, along with the two decay parameters,  $\alpha_-$  and  $\alpha_+$ , have already been precisely measured using the same data set in Refs. [44, 45]. Therefore, the free physics parameters in  $\omega$  are reduced to three from six – the couplings  $g_{av}$ ,  $g_w$  and  $g_{av2}$ . These couplings can therefore be determined with optimal precision, even with a relatively modest data sample. The details of the maximum log-likelihood fit procedure and the systematic uncertainties are described in Methods.

The final results for the axial vector and weak magnetism couplings are summarized in Table 1. They are determined separately for the  $e^\pm$  semi-leptonic channels and simultaneously by assuming  $g_i^- = -g_i^+$ ,  $i = \{av, av2\}$ , and  $g_w^- = g_w^+$ . Two results are provided: one where the weak electricity coupling is fixed to the SU(3) symmetry limit [9, 34],  $g_{av2} = 0$ , and the other where it is determined along with the other two couplings. The first result allows for a more precise extraction of  $g_{av}$  and  $g_w$ . The value of the weak magnetism coupling,  $\langle g_w \rangle = 0.89 \pm 0.38$ , is consistent with both the conserved vector current hypothesis prediction of 0.97 [35] and previous measurement of  $g_w = 0.15 \pm 0.30$  [12], with the latter agreement at the  $1.5\sigma$  level. For the second set, the weak electricity coupling is found to be  $\langle g_{av2} \rangle = -0.19^{+0.65}_{-0.63}$  providing the first measurement for  $\Lambda$   $\beta$  decay. It is also three times more precise compared to the KTeV determination of  $g_{av2}$  for the  $\Xi^0 \rightarrow \Sigma^+$  semi-leptonic decay [33]. The corresponding results for the average axial-vector and weak magnetism couplings are  $\langle g_{av} \rangle = 0.706^{+0.089}_{-0.086}$  and  $\langle g_w \rangle = 0.77^{+0.53}_{-0.49}$  and agree with the first set within the uncertainties.

To extract the CKM matrix element  $|V_{us}|$  from equation (1) we use the  $\Lambda$  lifetime  $\tau_\Lambda = (2.617 \pm 0.010) \cdot 10^{-10}$  s [8], and our determined  $\langle g_{av} \rangle$ ,  $\langle g_w \rangle$  and  $\mathcal{B}(\Lambda \rightarrow pe^-\bar{\nu}_e)$ . Meanwhile, we assume  $g_2 = 0$  [9], which is consistent with our second set of form factor results and also assumed by the previous experimental measurements [11, 12, 46] and for the determination of  $|V_{us}|$  [9, 34]. The term  $O(\beta^3)$  is ignored as its contribution is negligible within current experimental accuracy. For the decay rate one also needs to account for radiative effects, which modifies the decay rate by  $(1.6 \pm 0.5) \cdot 10^{-2}$  [47].

The final hurdle before obtaining  $|V_{us}|$  is that either  $f_1$  or  $g_1$  must be explicitly provided, either from theory or lattice QCD. This is similar to kaon semi-leptonic decays, where

**Table 1 Summary of the results .**

| Observable   | This work                                 | Previous result                  | Refs.   |
|--|---|----------------------------------|---------|
| $\mathcal{B}(\Lambda \rightarrow pe^-\bar{\nu}_e)$ | $(8.16 \pm 0.22 \pm 0.15) \times 10^{-4}$ | $(8.34 \pm 0.14) \times 10^{-4}$ | [8]     |
| $g_{av}^-$   | $0.742^{+0.075}_{-0.057} \pm 0.009$       | $0.718 \pm 0.015$                | [8]     |
| $g_{av}^+$   | $-0.706^{+0.069}_{-0.073} \pm 0.014$      | —                                |         |
| $\langle g_{av} \rangle$                           | $0.729^{+0.048}_{-0.047} \pm 0.007$       | —                                |         |
| $g_w^-$  | $0.93 \pm 0.51 \pm 0.17$                  | $0.15 \pm 0.30$                  | [12]    |
| $g_w^+$  | $0.89 \pm 0.49 \pm 0.20$                  | —                                |         |
| $\langle g_w \rangle$                              | $0.89 \pm 0.35 \pm 0.14$                  | —                                |         |
| $ V_{us} _{\text{SU}(3)}$                          | $0.2199 \pm 0.0094$                       | $0.2224 \pm 0.0034$              | [9, 34] |
| $ V_{us} _{\text{LQCD}}$                           | $0.2332 \pm 0.0042$                       |                                  |         |
| $ V_{us}  \cdot \sqrt{f_1^2 + 3g_1^2}$             | $0.4543 \pm 0.0076$                       | —                                |         |
| $\langle g_{av} \rangle$                           | $0.706^{+0.089}_{-0.086}$                 | —                                |         |
| $\langle g_w \rangle$                              | $0.77^{+0.53}_{-0.49}$                    | —                                |         |
| $\langle g_{av2} \rangle$                          | $-0.19^{+0.65}_{-0.63}$                   | —                                |         |

The branching fraction  $\mathcal{B}$  of  $\Lambda \rightarrow pe^-\bar{\nu}_e$  and form factor ratios for  $\Lambda \rightarrow pe^-\bar{\nu}_e (g_{av}^-, g_w^-)$ ,  $\bar{\Lambda} \rightarrow \bar{p}e^+\nu_e (g_{av}^+, g_w^+)$  and the average  $\langle g_{av} \rangle$  and  $\langle g_w \rangle$  with the constraint that  $g_{av2} = 0$ , where the first and second uncertainties are statistical and systematic, respectively; the value of  $|V_{us}|$  within the SU(3) symmetry limit and with the lattice QCD prediction, the product of the  $|V_{us}|$  and the form factors  $|V_{us}| \cdot \sqrt{f_1^2 + 3g_1^2}$ , where the uncertainties are total **systematic** uncertainties calculated as a sum in quadrature of the individual **systematic** uncertainties; the average  $\langle g_{av} \rangle$  and  $\langle g_w \rangle$  with the average  $\langle g_{av2} \rangle$  result with statistical uncertainties.

the corresponding form factor  $f_+$  is required as input [8]. As a reference value for our discussions, we assume that flavour SU(3) symmetry is conserved. Under this assumption,  $f_1$  takes on the value  $-\sqrt{3/2}$  [9] and  $|V_{us}|_{\text{SU}(3)} = 0.2199 \pm 0.0036_{\text{BESIII BF}} \pm 0.0087_{\text{BESIII FF}} \pm 0.0004_{\tau_\Lambda} \pm 0.0005_{\text{RC}}$ . The first and second uncertainties are from our measurements of the branching fraction and form factors, respectively, the third from the  $\Lambda$  lifetime, while the fourth is the radiative correction uncertainties [47]. This result is in good agreement with the value extracted by Cabibbo from the  $\Lambda \rightarrow pe^-\bar{\nu}_e$  world average,  $|V_{us}| = 0.2224 \pm 0.0034$  [9]. The value is also consistent with the CKM unitarity requirement within 0.8 standard deviations,  $|V_{us}| = 0.22799 \pm 0.00137$  [8, 48]. Various theoretical models account for the potential effects of flavor SU(3) symmetry-breaking, therefore we require a more accurate input which reflects this fact. Recent lattice QCD calculation [27] provides the first complete determination of the form factors including their  $q^2$  dependence. This allows to use the measured by us  $\mathcal{B}(\Lambda \rightarrow pe^-\bar{\nu}_e)$  with the  $\beta^7$  order expression for the decay rate (Eq. 40 of [27]) to obtain  $|V_{us}|_{\text{LQCD}} = 0.2332 \pm 0.0039_{\text{BESIII BF}} \pm 0.0004_{\tau_\Lambda} \pm 0.0006_{\text{RC}} \pm 0.0014_{\text{LQCD}}$ , where the fourth uncertainty arises from the lattice QCD prediction. The total uncertainty is currently dominated by the statcal uncertainty in the branching fraction measurement. The combined result from BESIII and lattice QCD,  $|V_{us}|_{\text{LQCD}}$ , is consistent with CKM unitarity at the  $1.2\sigma$  level, however, it is approximately  $2\sigma$  larger than from Cabibbo's method [9, 34] as shown in Fig. 4.

The pie chart in Fig. 4 shows the contributing uncertainties of this measurement. The form factor contribution (11.2%) can still be significantly reduced by further calculations from

lattice QCD. The statistical uncertainty of the branching fraction, 0.0032, is the dominant experimental uncertainty on  $|V_{us}|$ .

Additionally the product of  $|V_{us}|$  and the form factors at zero momentum transfer,  $q^2 = 0$ , has been extracted  $|V_{us}| \cdot \sqrt{f_1^2 + 3g_1^2} = 0.4543 \pm 0.0062_{\text{BESIII BF}_{\text{stat}}} \pm 0.0042_{\text{BESIII BF}_{\text{syst}}} \pm 0.0009_{\tau_\Lambda} \pm 0.0011_{\text{RC}}$ , where the dominant contribution from the form factors is included. This marks the first determination of such a product for any semi-leptonic baryon decay. Notably, the result is model-independent, as it avoids reliance on theoretical form factor predictions, thereby offering stringent constraints for testing and refining theoretical models.

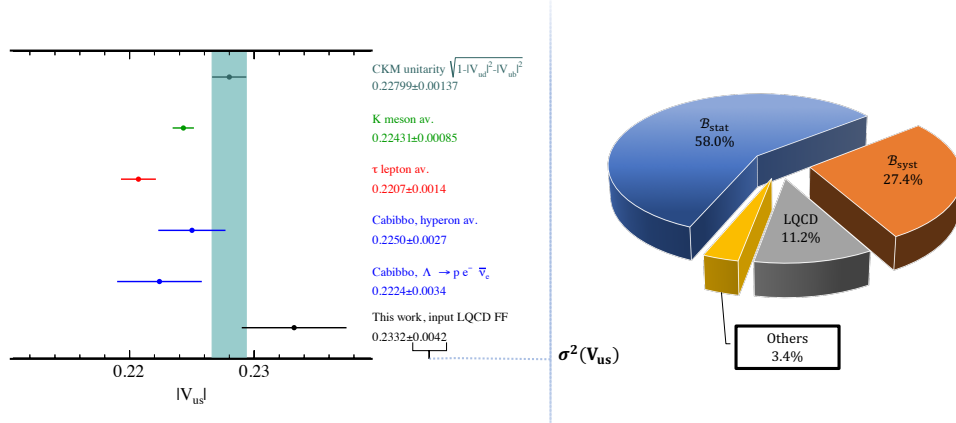


**Fig. 4 The  $|V_{us}|$  result.** (left) The first-row CKM unitarity constraint and  $K$  average are from Ref. [8]. The  $\tau$  average is from the Heavy Flavor Averaging Group [48]. The two hyperon results were evaluated by Cabibbo in [9, 34]. (right) The contributing sources to the  $|V_{us}|$  uncertainty, in terms of the variance.

Summarizing our findings, using spin-entangled and polarized strange baryon–antibaryon pairs we have reported the first absolute branching fraction determination for the semi-leptonic  $e$ -mode of strange baryon decays. We have determined the parameters related to internal structure — the axial-vector coupling  $g_{av}$  and weak magnetism coupling  $g_w$  of  $\Lambda \beta$  decay. Additionally, we have performed the first measurement of the weak electricity coupling  $g_{av2}$  for the  $\Lambda$  baryon. We obtain two values for  $|V_{us}|$ : one of which uses the normalization based on the SU(3) symmetry [49], and the other incorporates lattice QCD calculations as additional input [27]. This is the first experimental input for the  $|V_{us}|$  determination after a more than thirty years break for the study of semileptonic  $\Lambda$  decay. The novel modular approach [38], that allows to extract the measured parameters with reasonable uncertainties with a limited data set, has been applied in the analysis. Although the uncertainties are still limited by the sample size, we show how the lattice QCD input can significantly improve the precision in the determination of the CKM matrix element using hyperon semileptonic decays. The form factors of the semileptonic decays are interrelated and means that our method can be used and combined with other hyperon decays. Together with lattice input, it would therefore allow for an extraction of  $|V_{us}|$  with a sensitivity comparable to that of kaon decays. Furthermore, the analysis method is directly applicable to other baryon semileptonic

decays at BESIII and other present and future particle-antiparticle collider facilities such as the upcoming PANDA experiment [50] and the proposed Super Tau-Charm Factories [51, 52].

## References

- [1] Hofstadter, R. & McAllister, R. W. Electron Scattering From the Proton. Phys. Rev. **98**, 217–218 (1955).
- [2] Gao, H. & Vanderhaeghen, M. The proton charge radius. Rev. Mod. Phys. **94**, 015002 (2022).
- [3] Bernard, V., Elouadrhiri, L. & Meissner, U.-G. Axial structure of the nucleon: Topical Review. J. Phys. G **28**, R1–R35 (2002).
- [4] Cai, T. et al. Measurement of the axial vector form factor from antineutrino–proton scattering. Nature **614**, 48–53 (2023).
- [5] Chang, C. C. et al. A percent-level determination of the nucleon axial coupling from quantum chromodynamics. Nature **558**, 91–94 (2018).
- [6] Seng, C.-Y., Galviz, D., Marciano, W. J. & Meißner, U.-G. Update on  $|V_{us}|$  and  $|V_{us}/V_{ud}|$  from semileptonic kaon and pion decays. Phys. Rev. D **105**, 013005 (2022).
- [7] Garcia, A. & Kielanowski, P. The Beta Decay of Hyperons. Lect.Notes Phys. **222**, 1–173 (1985).
- [8] Navas, S. et al. Review of particle physics. Phys. Rev. D **110**, 030001 (2024).
- [9] Cabibbo, N., Swallow, E. C. & Winston, R. Semileptonic hyperon decays. Ann. Rev. Nucl. Part. Sci. **53**, 39–75 (2003).
- [10] Wise, J. et al. Precise Measurement of  $\Gamma(\Lambda \rightarrow pe^-\bar{\nu}_e)/\Gamma(\Lambda \rightarrow p\pi^-)$ . Phys. Lett. B **91**, 165–168 (1980).
- [11] Bourquin, M. et al. Measurements of Hyperon Semileptonic Decays at the CERN Super Proton Synchrotron. 2. The  $\Lambda \rightarrow pe^-\bar{\nu}_e$ ,  $\Xi^- \rightarrow \Lambda e^-\bar{\nu}_e$ , and  $\Xi^- \rightarrow \Sigma^0 e^-\bar{\nu}_e$  Decay Modes. Z. Phys. C **21**, 1 (1983).
- [12] Dworkin, J. et al. High statistics measurement of  $g_a/g_v$  in  $\Lambda \rightarrow pe^-\bar{\nu}_e$ . Phys. Rev. D **41**, 780–800 (1990).
- [13] Ademollo, M. & Gatto, R. Nonrenormalization Theorem for the Strangeness Violating Vector Currents. Phys. Rev. Lett. **13**, 264–265 (1964).
- [14] Donoghue, J. F., Holstein, B. R. & Klimt, S. W. K-m Angles and SU(3) Breaking in Hyperon beta Decay. Phys. Rev. D **35**, 934 (1987).

- [15] Schlumpf, F. Beta decay of hyperons in a relativistic quark model. Phys. Rev. D **51**, 2262–2270 (1995).
- [16] Flores-Mendieta, R., Jenkins, E. E. & Manohar, A. V. SU(3) symmetry breaking in hyperon semileptonic decays. Phys. Rev. D **58**, 094028 (1998).
- [17] Flores-Mendieta, R.  $V_{us}$  from hyperon semileptonic decays. Phys. Rev. D **70**, 114036 (2004).
- [18] Flores-Mendieta, R. & Sanchez-Almanza, G. Universality of the baryon axial vector current operator in large- $N_c$  chiral perturbation theory (2024).
- [19] Flores-Mendieta, R. & Sanchez-Almanza, G. Leading vector coupling in baryon semileptonic decays in large- $N_c$  chiral perturbation theory revisited: Extension to decuplet baryons (2025).
- [20] Krause, A. Baryon Matrix Elements of the Vector Current in Chiral Perturbation Theory. Helv. Phys. Acta **63**, 3–70 (1990).
- [21] Anderson, J. & Luty, M. A. Chiral corrections to hyperon vector form-factors. Phys. Rev. D **47**, 4975–4980 (1993).
- [22] Kaiser, N. Isospin breaking in neutron beta decay and SU(3) violation in semileptonic hyperon decays. Phys. Rev. C **64**, 028201 (2001).
- [23] Zhang, S.-Q., Zhang, X.-H. & Qiao, C.-F. Hyperon semileptonic decays in QCD sum rules. JHEP **06**, 122 (2024).
- [24] Mateu, V. & Pich, A.  $V_{us}$  determination from hyperon semileptonic decays. JHEP **10**, 041 (2005).
- [25] Guadagnoli, D. et al. Chiral extrapolation of hyperon vector form-factors. PoS LAT2005, 358 (2006).
- [26] Guadagnoli, D., Lubicz, V., Papinutto, M. & Simula, S. First Lattice QCD Study of the  $\Sigma^- \rightarrow n$  Axial and Vector Form Factors with SU(3) Breaking Corrections. Nucl. Phys. B **761**, 63–91 (2007).
- [27] Bacchio, S. & Konstantinou, A. Study of the  $\Lambda \rightarrow p\ell\bar{\nu}_\ell$  semileptonic decay in lattice QCD (2025). [2507.09970](#).
- [28] Guadagnoli, D., Martinelli, G., Papinutto, M. & Simula, S. Semileptonic hyperon decays on the Lattice: An Exploratory study. Nucl. Phys. B Proc. Suppl. **140**, 390–392 (2005).
- [29] Hashimoto, S. et al. Lattice QCD calculation of  $\bar{B} \rightarrow D\bar{\nu}$  decay form-factors at zero recoil. Phys. Rev. D **61**, 014502 (1999).

- [30] Becirevic, D. et al. The  $K \rightarrow \pi$  vector form-factor at zero momentum transfer on the lattice. *Nucl. Phys. B* **705**, 339–362 (2005).
- [31] Erkol, G., Oka, M. & Takahashi, T. T. Axial Charges of Octet Baryons in Two-flavor Lattice QCD. *Phys. Lett. B* **686**, 36–40 (2010).
- [32] Alvarez-Ruso, L. et al. NuSTEC White Paper: Status and challenges of neutrino–nucleus scattering. *Prog. Part. Nucl. Phys.* **100**, 1–68 (2018).
- [33] Alavi-Harati, A. et al. First Measurement of Form-Factors of the Decay  $\Xi^0 \rightarrow \Sigma^+ e^- \bar{\nu}_e$ . *Phys. Rev. Lett.* **87**, 132001 (2001).
- [34] Cabibbo, N., Swallow, E. C. & Winston, R. Semileptonic hyperon decays and CKM unitarity. *Phys. Rev. Lett.* **92**, 251803 (2004).
- [35] Gell-Mann, M. & Levy, M. The axial vector current in beta decay. *Nuovo Cim.* **16**, 705 (1960).
- [36] Aoki, Y. et al. FLAG Review 2021. *Eur. Phys. J. C* **82**, 869 (2022).
- [37] Perotti, E., Fäldt, G., Kupsc, A., Leupold, S. & Song, J. J. Polarization observables in  $e^+e^-$  annihilation to a baryon-antibaryon pair. *Phys. Rev. D* **99**, 056008 (2019).
- [38] Batzskaya, V., Kupsc, A., Salone, N. & Wiechnik, J. Semileptonic decays of spin-entangled baryon-antibaryon pairs. *Phys. Rev. D* **108**, 016011 (2023).
- [39] Ablikim, M. et al. Number of  $J/\psi$  events at BESIII. *Chin. Phys. C* **46**, 074001 (2022).
- [40] Verkerke, W. & Kirkby, D. P. The RooFit toolkit for data modeling. *eConf C0303241*, MOLT007 (2003).
- [41] Baltrusaitis, R. M. et al. Direct Measurements of Charmed d Meson Hadronic Branching Fractions. *Phys. Rev. Lett.* **56**, 2140 (1986).
- [42] Ge, J. Y. et al. Study of  $D^0 \rightarrow \pi^- e^+ \nu_e$ ,  $D^+ \rightarrow \pi^0 e^+ \nu_e$ ,  $D^0 \rightarrow K^- e^+ \nu_e$ , and  $D^+ \rightarrow \bar{K}^0 e^+ \nu_e$  in Tagged Decays of the  $\psi(3770)$  Resonance. *Phys. Rev. D* **79**, 052010 (2009).
- [43] Ablikim, M. et al. First Measurement of the Absolute Branching Fraction of  $\Lambda \rightarrow p \mu^- \bar{\nu}_\mu$ . *Phys. Rev. Lett.* **127**, 121802 (2021).
- [44] Ablikim, M. et al. Polarization and Entanglement in Baryon-Antibaryon Pair Production in Electron-Positron Annihilation. *Nature Phys.* **15**, 631–634 (2019).
- [45] Ablikim, M. et al. Precise Measurements of Decay Parameters and  $CP$  Asymmetry with Entangled  $\Lambda - \bar{\Lambda}$  Pairs. *Phys. Rev. Lett.* **129**, 131801 (2022).
- [46] Wise, J. et al. Precise Measurement of the Ratio of the Axial Vector Coupling to Vector Coupling in  $\Lambda^0 \rightarrow p e^- \bar{\nu}$ . *Phys. Lett. B* **98**, 123 (1981). [Erratum: *Phys. Lett. B* 100, 519

- (1981)].
- [47] Flores-Mendieta, R., Garcia, A., Martinez, A. & Torres, J. J. Radiative corrections to the semileptonic Dalitz plot with angular correlation between polarized decaying and emitted hyperons. Phys. Rev. D **55**, 5702–5718 (1997).
  - [48] Amhis, Y. S. et al. Averages of b-hadron, c-hadron, and  $\tau$ -lepton properties as of 2021. Phys. Rev. D **107**, 052008 (2023).
  - [49] Cabibbo, N. Unitary Symmetry and Leptonic Decays. Phys. Rev. Lett. **10**, 531–533 (1963).
  - [50] Barucca, G. et al. The potential of  $\Lambda$  and  $\Xi^-$  studies with PANDA at FAIR. Eur. Phys. J. A **57**, 154 (2021).
  - [51] Achasov, M. et al. STCF conceptual design report (Volume 1): Physics & detector. Front. Phys. (Beijing) **19**, 14701 (2024).
  - [52] Barnyakov, A. Y. The project of the Super Charm-Tau Factory in Novosibirsk. J. Phys. Conf. Ser. **1561**, 012004 (2020).
  - [53] Ablikim, M. et al. Design and Construction of the BESIII Detector. Nucl. Instrum. Meth. A **614**, 345–399 (2010).
  - [54] Yu, C. et al. BEPCII Performance and Beam Dynamics Studies on Luminosity, TUYA01 (JACoW Publishing, 2016).
  - [55] Agostinelli, S. et al. GEANT4—a simulation toolkit. Nucl. Instrum. Meth. A **506**, 250–303 (2003).
  - [56] Jadach, S., Ward, B. F. L. & Was, Z. Coherent exclusive exponentiation for precision Monte Carlo calculations. Phys. Rev. D **63**, 113009 (2001).
  - [57] Lange, D. J. The EvtGen particle decay simulation package. Nucl. Instrum. Meth. A **462**, 152–155 (2001).
  - [58] Yang, R.-L., Ping, R.-G. & Chen, H. Tuning and Validation of the Lundcharm Model with  $J/\psi$  Decays. Chin. Phys. Lett. **31**, 061301 (2014).
  - [59] Richter-Was, E. QED bremsstrahlung in semileptonic B and leptonic tau decays. Phys. Lett. B **303**, 163–169 (1993).
  - [60] James, F. & Roos, M. Minuit: A System for Function Minimization and Analysis of the Parameter Errors and Correlations. Comput. Phys. Commun. **10**, 343–367 (1975).
  - [61] Kadeer, A., Korner, J. G. & Moosbrugger, U. Helicity analysis of semileptonic hyperon decays including lepton mass effects. Eur. Phys. J. C **59**, 27–47 (2009).

- [62] Korner, J. G. & Kuroda, M.  $e^+e^-$  Annihilation Into Baryon-anti-Baryon Pairs. Phys. Rev. D **16**, 2165 (1977).
- [63] Feldmann, T. & Yip, M. W. Y. Form factors for  $\Lambda_b \rightarrow \Lambda$  transitions in the soft-collinear effective theory. Phys. Rev. D **85**, 014035 (2012). [Erratum: Phys. Rev. D **86**, 079901 (2012)].
- [64] Ablikim, M. et al. Search for hadronic transition  $\chi_{cJ} \rightarrow \eta_c \pi^+ \pi^-$  and observation of  $\chi_{cJ} \rightarrow K\bar{K}\pi\pi$ . Phys. Rev. D **87**, 012002 (2013).
- [65] Faustov, R. N. & Galkin, V. O. Rare  $\Lambda_c \rightarrow p\ell^+\ell^-$  decay in the relativistic quark model. Eur. Phys. J. C **78**, 527 (2018).

## Methods

### Experimental Apparatus

The BESIII detector [53] records symmetric  $e^+e^-$  collisions provided by the BEPCII storage ring [54]. In this cylindrical system, tracks of charged particles in the detector are reconstructed from track-induced signals and their momenta are determined from the track curvature in the multilayer drift chamber (MDC). The flight time of the charged particles are recorded by a plastic scintillator time-of-flight subdetectors (TOF). Electromagnetic showers from photons are reconstructed in the electromagnetic calorimeter (EMC). More details about the design and performance of the BESIII detector are found in Ref. [53].

### Monte Carlo Simulation

For the selection, efficiency determination and background evaluation of the single and double tag processes, Monte Carlo (MC) simulations have been used. The GEANT4-based package [55] includes the geometric description and detector response of the BESIII detector. The inclusive MC sample includes both the production of the  $J/\psi$  resonance and the continuum processes incorporated in the KKMC simulation package [56]. All particle decays are modelled with EVTGEN [57] using the branching fractions from the Particle Data Group when available [8], or else estimated with LUNDCHARM [58]. Final state radiation of the charged final state particles are simulated with PHOTOS [59]. The inclusive MC sample does not consider the decay dynamics and is thus only used for qualitative background studies. For the signal channel  $J/\psi \rightarrow \Lambda(\rightarrow pe^-\bar{\nu}_e)\bar{\Lambda}(\rightarrow \bar{p}\pi^+) + c.c.$  and the background,  $J/\psi \rightarrow \Lambda(\rightarrow p\pi^+)\bar{\Lambda}(\rightarrow \bar{p}\pi^+)$  dedicated MC samples were produced. In addition, these two modes include realistic production and decay dynamics using the physics parameter values in agreement with the results in Table 1, and in Ref. [44].

### Event selection criteria

For the single-tagged  $\bar{\Lambda}(\Lambda)$  sample, the same selection procedure is applied as in Ref. [43]. The double tag candidates are selected from the remaining tracks recoiling with respect to the ST candidates. All charged tracks must satisfy  $|\cos\theta_{\text{LAB}}| < 0.93$ , where  $\theta$  is defined with respect to the  $z$ -axis, which is the symmetry axis of the MDC. Only events with four charged

tracks are considered further. For the  $\Lambda$  reconstruction, the pair of charged tracks is constrained to originate from a common vertex. Furthermore, the decay length of the  $\Lambda$  candidate is required to be greater than zero. To identify whether a charged track is an electron/positron or a pion, particle identification (PID) is required. Each track is assigned a likelihood based on the MDC ionization energy loss and information from the TOF and EMC sub-systems. The other track is assumed to be a proton. After these requirements have been imposed on the data set, there is still a sizable contribution from the non-leptonic  $\Lambda \rightarrow p\pi^-$  decay. To suppress these events, we assume that the DT semi-leptonic candidates are in fact the hadronic decay but with a misidentified electron. This modifies the  $\Lambda$  decay vertex which in turn also modifies the  $\Lambda$  momentum vector. Then a four constraint kinematic fit (4C-fit) is imposed, which tests energy and momentum conservation in the  $J/\psi \rightarrow \Lambda\bar{\Lambda}$  hypothesis. If the  $\chi^2$  of the 4C-fit is lower than fifty, then the event is more likely to be a background and hence discarded. The  $\chi^2_{4C}$  selection removes  $84.4 \pm 0.2\%$  and  $4.30 \pm 0.02\%$  of the background and signal components, respectively. Except for  $\Lambda \rightarrow p\pi^-$ , we find no other source of peaking background. A potential background that includes an extra photon,  $\Lambda \rightarrow p\pi^-\gamma$  decay, was also studied with an exclusive MC simulation. Its contribution was found to be negligible, only 0.02%.

To improve the data quality the electron momentum is required to be larger than  $0.1 \text{ GeV}/c^2$ . Since the neutrino is undetected, the kinematic variable  $U_{\text{miss}} \equiv E_{\text{miss}} - c|\vec{p}_{\text{miss}}|$ , is introduced. Here,  $E_{\text{miss}}$  and  $\vec{p}_{\text{miss}}$  are the missing energy and momentum carried by the neutrino, respectively. These are calculated from  $E_{\text{miss}} = E_{\text{beam}} - E_p - E_{e^-}$  and  $\vec{p}_{\text{miss}} = \vec{p}_\Lambda - \vec{p}_p - \vec{p}_{e^-}$ , respectively, where  $E_{\text{beam}}$  is the beam energy,  $E_{p(e^-)}$  and  $\vec{p}_{p(e^-)}$  are the measured energies and momentum of the proton (electron), respectively. To determine the  $\Lambda$  momentum,  $\vec{p}_\Lambda$ , the momentum and magnitude from the produced  $\bar{\Lambda}$  partner combined with the known beam energy are used. For the signal candidates, the  $U_{\text{miss}}$  distribution is expected to peak around zero. The four-momentum transfer  $q^2$  is determined as  $q^2 = (E_{\text{beam}} - E_p)^2 - (\vec{p}_\Lambda - \vec{p}_p)^2$ .

#### Definition of the helicity amplitudes

In the  $e^+e^- \rightarrow \Lambda(\rightarrow pe^-\bar{\nu}_e)\bar{\Lambda}(\rightarrow \bar{p}\pi^+)$  process, the ‘master coordinate system’, denoted  $\mathcal{R}$ , is defined in the  $e^+e^-$  centre-of-momentum system. In this system, we define the unit vector  $\hat{z}$  in the direction of the positron momentum. The coordinate system  $\mathcal{R}_\Lambda$  is then defined in the rest frame of the  $\Lambda$  baryon, with the  $z$  axis along the unit vector  $\hat{z}_\Lambda$  defined by the direction of the  $\Lambda$  momentum in the  $\mathcal{R}$  system. A Cartesian coordinate system with  $\hat{x}_\Lambda$  and  $\hat{y}_\Lambda$  unit vectors is defined as

$$\hat{x}_\Lambda = \frac{\hat{z} \times \hat{z}_\Lambda}{|\hat{z} \times \hat{z}_\Lambda|} \times \hat{z}_\Lambda, \quad \hat{y}_\Lambda = \frac{\hat{z} \times \hat{z}_\Lambda}{|\hat{z} \times \hat{z}_\Lambda|}. \quad (4)$$

The helicity system  $\mathcal{R}_{\bar{\Lambda}}$  is defined in the same way in the  $\bar{\Lambda}$  rest frame, and because  $\hat{z}_\Lambda = -\hat{z}_{\bar{\Lambda}}$ .

#### The maximum log-likelihood fit procedure

A simultaneous fit is performed to the two c.c. channels,  $J/\psi \rightarrow \Lambda(\rightarrow pe^-\bar{\nu}_e)\bar{\Lambda}(\rightarrow \bar{p}\pi^+)$  and  $J/\psi \rightarrow \Lambda(\rightarrow p\pi^-)\bar{\Lambda}(\rightarrow \bar{p}e^+\nu_e)$ . At this level of precision charge parity (CP) is a conserved symmetry, so these CP-odd relations are valid:  $\alpha_- = -\alpha_+$ ,  $g_{av}^- = -g_{av}^+$ ,  $g_w^- = g_w^+$  and  $g_{av2}^- = -g_{av2}^+$  which reduces the number of free parameters in  $\xi$ . For  $N$  number of experimental events the likelihood, constructed from the probability density function for an event characterized

by  $\xi_i$  is

$$\mathcal{L} = \prod_{i=1}^N \mathcal{P}(\xi_i; \omega) = \prod_{i=1}^N \frac{\mathcal{W}(\xi_i; \omega) \varepsilon(\xi_i)}{\mathcal{N}(\omega)}, \quad (5)$$

where  $\varepsilon(\xi_i)$  is the detection efficiency, the normalization factor  $\mathcal{N}(\omega) = \int \mathcal{W}(\xi; \omega) \varepsilon(\xi) d\xi$  with weights  $\mathcal{W}(\xi; \omega)$  as specified in equation (2). The normalization factor is approximated as  $\mathcal{N}(\omega) = \frac{1}{M} \sum_{j=1}^M [\mathcal{W}(\xi_j; \omega) / \mathcal{W}(\xi_j; \omega_{\text{gen}})]$  using  $M$  Monte Carlo events  $\xi_j$  generated using the angular distribution of the full process (2) with fixed parameters  $\omega_{\text{gen}}$ , propagated through the detector and reconstructed in the same way as the experimental data.  $M$  is chosen to be much larger than  $N$ ; in this case the ratio is  $M/N = 470$ . To take into account the difference of detection efficiency between MC and data, the detection efficiency is corrected for the final state particles,  $p, \bar{p}, \pi^+, \pi^-, e^+$  and  $e^-$ . The correction factors are obtained using the control samples  $J/\psi \rightarrow p\bar{p}\pi^+\pi^-$  and  $e^+e^- \rightarrow e^+e^-\gamma$ , where the correlation between the charged particle momentum and its polar angle acceptances is taken into account.

To determine the parameters, the Minuit package from the CERN library is used [60]. The minimizing function is given by  $S = -\ln \mathcal{L}_{\text{data}} + \ln \mathcal{L}_{\text{bkg}}$ , where  $\mathcal{L}_{\text{data}}$  and  $\mathcal{L}_{\text{bkg}}$  represents the two likelihoods for the semi-leptonic modes and the background events. The background contribution is evaluated using simulated data. In addition, the operational conditions were slightly different for the four data taking periods, most notably in the nominal value of the magnetic field. For this reason, the likelihoods are evaluated separately for the four different run periods.

### The $|V_{us}|$ determination

The partial decay width for the  $\Lambda \rightarrow pe^-\bar{\nu}_e$  decay as written in Eq. (1) with

$$\mathcal{F}_2 = 3f_1^2 + 3f_1f_2 + 2f_2^2 + 6g_1^2 + 6g_2^2 + 21g_1g_2 \quad (6)$$

was used in the determinations of  $|V_{us}|$  decays using Cabibbo method [7, 9, 34]. Here, the  $q^2$  dependence of the form factors is not included. To test the systematic effects due to this approximation we include as given by Eq. (40) of [27] the  $O(q^2)$  terms of the  $f_1$  and  $g_1$  form factors expansion around  $q^2 = 0$ :

$$f_1(q^2) \approx f_1 \cdot \left(1 + \frac{\langle r_{f_1}^2 \rangle}{6} q^2\right) \text{ and } g_1(q^2) \approx g_1 \cdot \left(1 + \frac{\langle r_{g_1}^2 \rangle}{6} q^2\right). \quad (7)$$

The  $\langle r_{f_1}^2 \rangle$  and  $\langle r_{g_1}^2 \rangle$  parameters are derived from the dipole parameterization [61, 62]:

$$\langle r_j^2 \rangle = \frac{6}{m_j^2(m_j^2 + \alpha_R^{-1})}, \quad (8)$$

with the corresponding dominant pole masses  $m_{f_1} = m_{K^*(892)^0} = 0.892$  GeV and  $m_{g_1} = m_{K_1(1270)} = 1.273$  GeV [62]. The  $K^*(892)^0$  and  $K_1(1270)$  mesons are the lowest lying strange vector mesons with  $J^P = 1^-$  and  $1^+$  quantum numbers, respectively. The slope of the Regge

trajectory is taken as  $\alpha_R = 0.9 \text{ GeV}^{-2}$ . To minimize the correlation between the axial vector and weak electricity couplings, the helicity-based definition of form factors (further called "helicity form factors") [63],  $g_+$ ,  $g_\perp$ ,  $f_+$  and  $f_\perp$ , are used in the joint angular distribution, which are then transformed back to the original representation, Weinberg's classification of form factors, through the relationship at zero momentum transfer of

$$\begin{aligned} f_+ &= f_1, & f_\perp &= f_1 + (2 - \beta)f_2, \\ g_+ &= g_1, & g_\perp &= g_1 - \beta g_2. \end{aligned} \quad (9)$$

This has the effect that the statistical fit uncertainties are slightly asymmetrical. According to the study in Ref. [47], the decay width with radiative correction is

$$\Gamma^c = \Gamma \cdot (1 + Cr), \quad (10)$$

where  $Cr$  is the radiative correction factor to the decay rate, and it has been calculated to be  $Cr = (1.6 \pm 0.5)\%$  for the decay  $\Lambda \rightarrow pe^- \bar{\nu}_e$  [47]. We use two approaches to determine  $|V_{us}|$ . The first is based on Eq. 1, employing the measured by us form factors  $\langle g_{av} \rangle$  and  $\langle g_w \rangle$  while fixing  $f_1$  and  $g_{av2}$  by assuming the SU(3) symmetry conservation. The second and the main result incorporates the full set of the form factors calculated in lattice QCD [27].

### Systematic uncertainties of branching fraction determination

Systematic studies have been performed separately for the branching fraction and form factors. For the branching fraction, the uncertainties arise from the requirement on the number of tracks and  $\Lambda$  vertex fit, the proton and electron detection, the 4C-fit, and the estimation of the number of candidates using ST and DT techniques.

**1. Requirement on the number of tracks and  $\Lambda$  vertex fit.** The control sample of  $J/\psi \rightarrow \Lambda(\rightarrow p\pi^-)\bar{\Lambda}(\rightarrow \bar{p}\pi^+)$  is used to study the systematic uncertainty due to the requirement of four final tracks and the  $\Lambda$  reconstruction through the vertex fit. For the requirement on the number of tracks, the MC efficiency is corrected by multiplying the correction factor obtained from the control sample, while the uncertainty from the correction factor is assigned as the systematic uncertainty. The systematic uncertainty due to the  $\Lambda$  vertex fit is assigned to be the efficiency difference between the data and MC.

**2.  $p$  and  $e^-$  detection.** To evaluate the systematic uncertainty from the track reconstruction of the protons and electrons, and their corresponding anti-particles, we use the two control channels  $J/\psi \rightarrow p\bar{p}\pi^-\pi^+$  and  $e^+e^- \rightarrow e^+e^-\gamma$ . From these, two-dimensional efficiency plots ( $\cos\theta_{\text{LAB}, p_T}$ ), one for each particle species is obtained. For each track, the efficiency plots are used to obtain a correction factor. For the proton, the difference between the nominal and track-corrected branching fraction is assigned to be the systematic uncertainty. For the electron, the uncertainty associated with the correction factor is assigned as the systematic uncertainty.

**3. Kinematic fit.** To test the better agreement of kinematic variables between data and MC samples, the simulated sample is corrected using the correction parameters for the charged tracks following procedure from [64]. The systematic uncertainty is assigned to be the difference between the fit results with and without the application of correction parameters.

**4. ST and DT techniques.** To test if the fit method produces systematically biased results,

**Table 2** Systematic uncertainty for the branching fraction measurement, relative to the central value, and the sum in quadrature.

| Source               | Uncertainty(%) |
|----------------------|----------------|
| Number of tracks     | 0.03           |
| $\Lambda$ vertex fit | 0.20           |
| $p$ tracking         | 0.26           |
| $e$ detection        | 1.55           |
| Kinematic fit        | 0.22           |
| ST fit method        | 0.37           |
| DT fit method        | 0.80           |
| Sum syst.            | 1.83           |

alternative fitting functions are used for the ST and DT variables. The difference between the main and alternative fit results is taken as the systematic uncertainty.

### Systematic uncertainties of form factor determination

Systematic uncertainties are assigned based on the electron momentum, parametrization of the  $q^2$  dependence, the estimator and the fit method. We also performed cross checks on the kinematic fit and decay length but found no significant systematic effect.

**1. Estimator.** To test if the method produces systematically biased results, a large Monte Carlo data sample is produced with production and decay distributions corresponding to those of the fit results to the data sample ( $\sim 400$  times the experimental data). The simulated data are divided into subsamples with equal number of events as the experimental sample, and run through the fit procedure, yielding distributions consisting of approximately 400 outputs. A Gaussian function is used to fit the output distribution of each form factor and the difference between the mean value of the fitted Gaussian function and generated parameter is assigned as systematic uncertainty.

**2. Parametrization of  $q^2$  dependence.** The bias on the form factor values due to the parametrization of the  $q^2$  dependence is evaluated using the relativistic quark model based on a quasipotential approach with a QCD-motivated potential (further called "z-expansion") with the number of poles equal to 0 [65]. The difference between the main fit result and the fit result with the z-expansion parametrization is found to be consistent within one standard deviation and hence no bias is assigned.

**3. Fit method.** The fit method introduces a systematic uncertainty from three different sources: fixed value of production and  $\alpha_+$  ( $\alpha_-$ ), parameters, number of background candidates from  $\Lambda \rightarrow p\pi^-$  and other sources, and MC efficiency correction factors. The contribution due to the uncertainty from these three sources is obtained by repeating the fit procedure 100 times after randomly varying all parameters within their uncertainties. A Gaussian function is used to fit each form factor and its width is taken as the systematic uncertainty.

**4.  $e^+$  and  $e^-$  momentum.** Possible systematic effects related to the electron and positron reconstruction are studied by varying the momentum selection criteria for the  $e^-$  and  $e^+$  candidates. The variation of results with changing selection criteria are seen for both cases which is accounted for in the final systematic uncertainty.

**Table 3** Contributing absolute systematic uncertainties to the form factor ratios, and the final sum, where the individual contributions are taken in quadrature. The first row shows the statistical uncertainty for reference.

|                 | $g_{av}^-$       | $g_w^-$          | $g_{av}^+$       | $g_w^+$          | $\langle g_{av} \rangle$ | $\langle g_w \rangle$ |
|-----------------|------------------|------------------|------------------|------------------|--------------------------|-----------------------|
| Statistical     | +0.075<br>-0.057 | +0.510<br>-0.506 | +0.069<br>-0.073 | +0.496<br>-0.486 | +0.048<br>-0.047         | +0.356<br>-0.353      |
| Estimator       | 0.001            | 0.007            | 0.004            | 0.003            | 0.001                    | 0.017                 |
| Fit method      | 0.004            | 0.148            | 0.012            | 0.183            | 0.006                    | 0.118                 |
| $p_e$ selection | 0.008            | 0.072            | 0.006            | 0.087            | 0.004                    | 0.067                 |
| Sum syst.       | 0.009            | 0.165            | 0.014            | 0.203            | 0.007                    | 0.137                 |

## The BESIII Collaboration

M. Ablikim<sup>1</sup>, M. N. Achasov<sup>4,c</sup>, P. Adlarson<sup>78</sup>, X. C. Ai<sup>83</sup>, R. Aliberti<sup>36</sup>, A. Amoroso<sup>77A,77C</sup>, Q. An<sup>74,60,a</sup>, Y. Bai<sup>58</sup>, O. Bakina<sup>37</sup>, Y. Ban<sup>47,h</sup>, H.-R. Bao<sup>66</sup>, V. Batozskaya<sup>1,45</sup>, K. Begzsuren<sup>33</sup>, N. Berger<sup>36</sup>, M. Berlowski<sup>45</sup>, M. Bertani<sup>29A</sup>, D. Bettoni<sup>30A</sup>, F. Bianchi<sup>77A,77C</sup>, E. Bianco<sup>77A,77C</sup>, A. Bortone<sup>77A,77C</sup>, I. Boyko<sup>37</sup>, R. A. Briere<sup>5</sup>, A. Brueggemann<sup>71</sup>, H. Cai<sup>79</sup>, M. H. Cai<sup>39,k,l</sup>, X. Cai<sup>1,60</sup>, A. Calcaterra<sup>29A</sup>, G. F. Cao<sup>1,66</sup>, N. Cao<sup>1,66</sup>, S. A. Cetin<sup>64A</sup>, X. Y. Chai<sup>47,h</sup>, J. F. Chang<sup>1,60</sup>, G. R. Che<sup>44</sup>, Y. Z. Che<sup>1,60,66</sup>, C. H. Chen<sup>9</sup>, Chao Chen<sup>56</sup>, G. Chen<sup>1</sup>, H. S. Chen<sup>1,66</sup>, H. Y. Chen<sup>21</sup>, M. L. Chen<sup>1,60,66</sup>, S. J. Chen<sup>43</sup>, S. L. Chen<sup>46</sup>, S. M. Chen<sup>63</sup>, T. Chen<sup>1,66</sup>, X. R. Chen<sup>32,66</sup>, X. T. Chen<sup>1,66</sup>, X. Y. Chen<sup>12,g</sup>, Y. B. Chen<sup>1,60</sup>, Y. Q. Chen<sup>35</sup>, Y. Q. Chen<sup>16</sup>, Z. Chen<sup>25</sup>, Z. J. Chen<sup>26,i</sup>, Z. K. Chen<sup>61</sup>, S. K. Choi<sup>10</sup>, X. Chu<sup>12,g</sup>, G. Cibinetto<sup>30A</sup>, F. Cossio<sup>77C</sup>, J. Cotee-Meldrum<sup>65</sup>, J. J. Cui<sup>51</sup>, H. L. Dai<sup>1,60</sup>, J. P. Dai<sup>81</sup>, A. Dbeyssi<sup>19</sup>, R. E. de Boer<sup>3</sup>, D. Dedovich<sup>37</sup>, C. Q. Deng<sup>75</sup>, Z. Y. Deng<sup>1</sup>, A. Denig<sup>36</sup>, I. Denysenko<sup>37</sup>, M. Destefanis<sup>77A,77C</sup>, F. De Mori<sup>77A,77C</sup>, B. Ding<sup>69,1</sup>, X. X. Ding<sup>47,h</sup>, Y. Ding<sup>41</sup>, Y. Ding<sup>35</sup>, Y. X. Ding<sup>31</sup>, J. Dong<sup>1,60</sup>, L. Y. Dong<sup>1,66</sup>, M. Y. Dong<sup>1,60,66</sup>, X. Dong<sup>79</sup>, M. C. Du<sup>1</sup>, S. X. Du<sup>83</sup>, S. X. Du<sup>12,g</sup>, Y. Y. Duan<sup>56</sup>, Z. H. Duan<sup>43</sup>, P. Egorov<sup>37,b</sup>, G. F. Fan<sup>43</sup>, J. J. Fan<sup>20</sup>, Y. H. Fan<sup>46</sup>, J. Fang<sup>1,60</sup>, J. Fang<sup>61</sup>, S. S. Fang<sup>1,66</sup>, W. X. Fang<sup>1</sup>, Y. Q. Fang<sup>1,60</sup>, L. Fava<sup>77B,77C</sup>, F. Feldbauer<sup>3</sup>, G. Felici<sup>29A</sup>, C. Q. Feng<sup>74,60</sup>, J. H. Feng<sup>16</sup>, L. Feng<sup>39,k,l</sup>, Q. X. Feng<sup>39,k,l</sup>, Y. T. Feng<sup>74,60</sup>, M. Fritsch<sup>3</sup>, C. D. Fu<sup>1</sup>, J. L. Fu<sup>66</sup>, Y. W. Fu<sup>1,66</sup>, H. Gao<sup>66</sup>, X. B. Gao<sup>42</sup>, Y. Gao<sup>74,60</sup>, Y. N. Gao<sup>20</sup>, Y. N. Gao<sup>47,h</sup>, Y. Y. Gao<sup>31</sup>, S. Garbolino<sup>77C</sup>, I. Garzia<sup>30A,30B</sup>, L. Ge<sup>58</sup>, P. T. Ge<sup>20</sup>, Z. W. Ge<sup>43</sup>, C. Geng<sup>61</sup>, E. M. Gersabeck<sup>70</sup>, A. Gilman<sup>72</sup>, K. Goetzen<sup>13</sup>, J. D. Gong<sup>35</sup>, L. Gong<sup>41</sup>, W. X. Gong<sup>1,60</sup>, W. Gradl<sup>36</sup>, S. Gramigna<sup>30A,30B</sup>, M. Greco<sup>77A,77C</sup>, M. H. Gu<sup>1,60</sup>, Y. T. Gu<sup>15</sup>, C. Y. Guan<sup>1,66</sup>, A. Q. Guo<sup>32</sup>, L. B. Guo<sup>42</sup>, M. J. Guo<sup>51</sup>, R. P. Guo<sup>50</sup>, Y. P. Guo<sup>12,g</sup>, A. Guskov<sup>37,b</sup>, J. Gutierrez<sup>28</sup>, K. L. Han<sup>66</sup>, T. T. Han<sup>1</sup>, F. Hanisch<sup>3</sup>, K. D. Hao<sup>74,60</sup>, X. Q. Hao<sup>20</sup>, F. A. Harris<sup>68</sup>, K. K. He<sup>56</sup>, K. L. He<sup>1,66</sup>, F. H. Heinsius<sup>3</sup>, C. H. Heinz<sup>36</sup>, Y. K. Heng<sup>1,60,66</sup>, C. Herold<sup>62</sup>, P. C. Hong<sup>35</sup>, G. Y. Hou<sup>1,66</sup>, X. T. Hou<sup>1,66</sup>, Y. R. Hou<sup>66</sup>, Z. L. Hou<sup>1</sup>, H. M. Hu<sup>1,66</sup>, J. F. Hu<sup>57,j</sup>, Q. P. Hu<sup>74,60</sup>, S. L. Hu<sup>12,g</sup>, T. Hu<sup>1,60,66</sup>, Y. Hu<sup>1</sup>, Z. M. Hu<sup>61</sup>, G. S. Huang<sup>74,60</sup>, K. X. Huang<sup>61</sup>, L. Q. Huang<sup>32,66</sup>, P. Huang<sup>43</sup>, X. T. Huang<sup>51</sup>, Y. P. Huang<sup>1</sup>, Y. S. Huang<sup>61</sup>, T. Hussain<sup>76</sup>, N. Hüsken<sup>36</sup>, N. in der Wiesche<sup>71</sup>, J. Jackson<sup>28</sup>, Q. Ji<sup>1</sup>, Q. P. Ji<sup>20</sup>, W. Ji<sup>1,66</sup>, X. B. Ji<sup>1,66</sup>, X. L. Ji<sup>1,60</sup>, Y. Y. Ji<sup>51</sup>, Z. K. Jia<sup>74,60</sup>, D. Jiang<sup>1,66</sup>, H. B. Jiang<sup>79</sup>, P. C. Jiang<sup>47,h</sup>, S. J. Jiang<sup>9</sup>, T. J. Jiang<sup>17</sup>, X. S. Jiang<sup>1,60,66</sup>, Y. Jiang<sup>66</sup>, J. B. Jiao<sup>51</sup>, J. K. Jiao<sup>35</sup>, Z. Jiao<sup>24</sup>, S. Jin<sup>43</sup>, Y. Jin<sup>69</sup>, M. Q. Jing<sup>1,66</sup>, X. M. Jing<sup>66</sup>, T. Johansson<sup>78</sup>, S. Kabana<sup>34</sup>, N. Kalantar-Nayestanaki<sup>67</sup>, X. L. Kang<sup>9</sup>, X. S. Kang<sup>41</sup>, M. Kavatsyuk<sup>67</sup>, B. C. Ke<sup>83</sup>, V. Khachatryan<sup>28</sup>, A. Khoukaz<sup>71</sup>, R. Kiuchi<sup>1</sup>, O. B. Kolcu<sup>64A</sup>, B. Kopf<sup>3</sup>, M. Kuessner<sup>3</sup>, X. Kui<sup>1,66</sup>, N. Kumar<sup>27</sup>, A. Kupsc<sup>45,78</sup>, W. Kühn<sup>38</sup>, Q. Lan<sup>75</sup>, W. N. Lan<sup>20</sup>, T. T. Lei<sup>74,60</sup>, M. Lellmann<sup>36</sup>, T. Lenz<sup>36</sup>, C. Li<sup>44</sup>, C. Li<sup>48</sup>, C. H. Li<sup>40</sup>, C. K. Li<sup>21</sup>, D. M. Li<sup>83</sup>, F. Li<sup>1,60</sup>, G. Li<sup>1</sup>, H. B. Li<sup>1,66</sup>, H. J. Li<sup>20</sup>, H. N. Li<sup>57,j</sup>, Hui Li<sup>44</sup>, J. R. Li<sup>63</sup>, J. S. Li<sup>61</sup>, K. Li<sup>1</sup>, K. L. Li<sup>39,k,l</sup>, K. L. Li<sup>20</sup>, L. J. Li<sup>1,66</sup>, Lei Li<sup>49</sup>, M. H. Li<sup>44</sup>, M. R. Li<sup>1,66</sup>, P. L. Li<sup>66</sup>, P. R. Li<sup>39,k,l</sup>, Q. M. Li<sup>1,66</sup>, Q. X. Li<sup>51</sup>, R. Li<sup>18,32</sup>, S. X. Li<sup>12</sup>, T. Li<sup>51</sup>, T. Y. Li<sup>44</sup>, W. D. Li<sup>1,66</sup>, W. G. Li<sup>1,a</sup>, X. Li<sup>1,66</sup>, X. H. Li<sup>74,60</sup>, X. L. Li<sup>51</sup>, X. Y. Li<sup>1,8</sup>, X. Z. Li<sup>61</sup>, Y. Li<sup>20</sup>, Y. G. Li<sup>47,h</sup>, Y. P. Li<sup>35</sup>, Z. J. Li<sup>61</sup>, Z. Y. Li<sup>81</sup>, C. Liang<sup>43</sup>, H. Liang<sup>74,60</sup>, Y. F. Liang<sup>55</sup>, Y. T. Liang<sup>32,66</sup>, G. R. Liao<sup>14</sup>, L. B. Liao<sup>61</sup>, M. H. Liao<sup>61</sup>, Y. P. Liao<sup>1,66</sup>, J. Libby<sup>27</sup>, A. Limphirat<sup>62</sup>, C. C. Lin<sup>56</sup>, D. X. Lin<sup>32,66</sup>, L. Q. Lin<sup>40</sup>, T. Lin<sup>1</sup>, B. J. Liu<sup>1</sup>, B. X. Liu<sup>79</sup>, C. Liu<sup>35</sup>, C. X. Liu<sup>1</sup>, F. Liu<sup>1</sup>, F. H. Liu<sup>54</sup>, Feng Liu<sup>6</sup>, G. M. Liu<sup>57,j</sup>, H. Liu<sup>39,k,l</sup>, H. B. Liu<sup>15</sup>, H. H. Liu<sup>1</sup>,

H. M. Liu<sup>1,66</sup>, Huihui Liu<sup>22</sup>, J. B. Liu<sup>74,60</sup>, J. J. Liu<sup>21</sup>, K. Liu<sup>75</sup>, K. Liu<sup>39,k,l</sup>, K. Y. Liu<sup>41</sup>, Ke Liu<sup>23</sup>, L. C. Liu<sup>44</sup>, Lu Liu<sup>44</sup>, M. H. Liu<sup>12,g</sup>, M. H. Liu<sup>35</sup>, P. L. Liu<sup>1</sup>, Q. Liu<sup>66</sup>, S. B. Liu<sup>74,60</sup>, T. Liu<sup>12,g</sup>, W. K. Liu<sup>44</sup>, W. M. Liu<sup>74,60</sup>, W. T. Liu<sup>40</sup>, X. Liu<sup>39,k,l</sup>, X. Liu<sup>40</sup>, X. K. Liu<sup>39,k,l</sup>, X. L. Liu<sup>12,g</sup>, X. Y. Liu<sup>79</sup>, Y. Liu<sup>39,k,l</sup>, Y. Liu<sup>83</sup>, Y. Liu<sup>83</sup>, Y. B. Liu<sup>44</sup>, Z. A. Liu<sup>1,60,66</sup>, Z. D. Liu<sup>9</sup>, Z. Q. Liu<sup>51</sup>, X. C. Lou<sup>1,60,66</sup>, F. X. Lu<sup>61</sup>, H. J. Lu<sup>24</sup>, J. G. Lu<sup>1,60</sup>, X. L. Lu<sup>16</sup>, Y. Lu<sup>7</sup>, Y. H. Lu<sup>1,66</sup>, Y. P. Lu<sup>1,60</sup>, Z. H. Lu<sup>1,66</sup>, C. L. Luo<sup>42</sup>, J. R. Luo<sup>61</sup>, J. S. Luo<sup>1,66</sup>, M. X. Luo<sup>82</sup>, T. Luo<sup>12,g</sup>, X. L. Luo<sup>1,60</sup>, Z. Y. Lv<sup>23</sup>, X. R. Lyu<sup>66,p</sup>, Y. F. Lyu<sup>44</sup>, Y. H. Lyu<sup>83</sup>, F. C. Ma<sup>41</sup>, H. L. Ma<sup>1</sup>, Heng Ma<sup>26,i</sup>, J. L. Ma<sup>1,66</sup>, L. L. Ma<sup>51</sup>, L. R. Ma<sup>69</sup>, Q. M. Ma<sup>1</sup>, R. Q. Ma<sup>1,66</sup>, R. Y. Ma<sup>20</sup>, T. Ma<sup>74,60</sup>, X. T. Ma<sup>1,66</sup>, X. Y. Ma<sup>1,60</sup>, Y. M. Ma<sup>32</sup>, F. E. Maas<sup>19</sup>, I. MacKay<sup>72</sup>, M. Maggiora<sup>77A,77C</sup>, S. Malde<sup>72</sup>, Q. A. Malik<sup>76</sup>, H. X. Mao<sup>39,k,l</sup>, Y. J. Mao<sup>47,h</sup>, Z. P. Mao<sup>1</sup>, S. Marcello<sup>77A,77C</sup>, A. Marshall<sup>65</sup>, F. M. Melendi<sup>30A,30B</sup>, Y. H. Meng<sup>66</sup>, Z. X. Meng<sup>69</sup>, G. Mezzadri<sup>30A</sup>, H. Miao<sup>1,66</sup>, T. J. Min<sup>43</sup>, R. E. Mitchell<sup>28</sup>, X. H. Mo<sup>1,60,66</sup>, B. Moses<sup>28</sup>, N. Yu. Muchnoi<sup>4,c</sup>, J. Muskalla<sup>36</sup>, Y. Nefedov<sup>37</sup>, F. Nerling<sup>19,e</sup>, L. S. Nie<sup>21</sup>, I. B. Nikolaev<sup>4,c</sup>, Z. Ning<sup>1,60</sup>, S. Nisar<sup>11,m</sup>, Q. L. Niu<sup>39,k,l</sup>, W. D. Niu<sup>12,g</sup>, C. Normand<sup>65</sup>, S. L. Olsen<sup>10,66</sup>, Q. Ouyang<sup>1,60,66</sup>, S. Pacetti<sup>29B,29C</sup>, X. Pan<sup>56</sup>, Y. Pan<sup>58</sup>, A. Pathak<sup>10</sup>, Y. P. Pei<sup>74,60</sup>, M. Pelizaeus<sup>3</sup>, H. P. Peng<sup>74,60</sup>, X. J. Peng<sup>39,k,l</sup>, Y. Y. Peng<sup>39,k,l</sup>, K. Peters<sup>13,e</sup>, K. Petridis<sup>65</sup>, J. L. Ping<sup>42</sup>, R. G. Ping<sup>1,66</sup>, S. Plura<sup>36</sup>, V. Prasad<sup>35</sup>, F. Z. Qi<sup>1</sup>, H. R. Qi<sup>63</sup>, M. Qi<sup>43</sup>, S. Qian<sup>1,60</sup>, W. B. Qian<sup>66</sup>, C. F. Qiao<sup>66</sup>, J. H. Qiao<sup>20</sup>, J. J. Qin<sup>75</sup>, J. L. Qin<sup>56</sup>, L. Q. Qin<sup>14</sup>, L. Y. Qin<sup>74,60</sup>, P. B. Qin<sup>75</sup>, X. P. Qin<sup>12,g</sup>, X. S. Qin<sup>51</sup>, Z. H. Qin<sup>1,60</sup>, J. F. Qiu<sup>1</sup>, Z. H. Qu<sup>75</sup>, J. Rademacker<sup>65</sup>, C. F. Redmer<sup>36</sup>, A. Rivetti<sup>77C</sup>, M. Rolo<sup>77C</sup>, G. Rong<sup>1,66</sup>, S. S. Rong<sup>1,66</sup>, F. Rosini<sup>29B,29C</sup>, Ch. Rosner<sup>19</sup>, M. Q. Ruan<sup>1,60</sup>, N. Salone<sup>45,q</sup>, A. Sarantsev<sup>37,d</sup>, Y. Schelhaas<sup>36</sup>, K. Schoenning<sup>78</sup>, M. Scodreggio<sup>30A</sup>, K. Y. Shan<sup>12,g</sup>, W. Shan<sup>25</sup>, X. Y. Shan<sup>74,60</sup>, Z. J. Shang<sup>39,k,l</sup>, J. F. Shangguan<sup>17</sup>, L. G. Shao<sup>1,66</sup>, M. Shao<sup>74,60</sup>, C. P. Shen<sup>12,g</sup>, H. F. Shen<sup>1,8</sup>, W. H. Shen<sup>66</sup>, X. Y. Shen<sup>1,66</sup>, B. A. Shi<sup>66</sup>, H. Shi<sup>74,60</sup>, J. L. Shi<sup>12,g</sup>, J. Y. Shi<sup>1</sup>, S. Y. Shi<sup>75</sup>, X. Shi<sup>1,60</sup>, H. L. Song<sup>74,60</sup>, J. J. Song<sup>20</sup>, T. Z. Song<sup>61</sup>, W. M. Song<sup>35</sup>, Y. J. Song<sup>12,g</sup>, Y. X. Song<sup>47,h,n</sup>, Zirong Song<sup>26,i</sup>, S. Sosio<sup>77A,77C</sup>, S. Spataro<sup>77A,77C</sup>, S. Stansilaus<sup>72</sup>, F. Stieler<sup>36</sup>, S. S. Su<sup>41</sup>, Y. J. Su<sup>66</sup>, G. B. Sun<sup>79</sup>, G. X. Sun<sup>1</sup>, H. Sun<sup>66</sup>, H. K. Sun<sup>1</sup>, J. F. Sun<sup>20</sup>, K. Sun<sup>63</sup>, L. Sun<sup>79</sup>, S. S. Sun<sup>1,66</sup>, T. Sun<sup>52,f</sup>, Y. C. Sun<sup>79</sup>, Y. H. Sun<sup>31</sup>, Y. J. Sun<sup>74,60</sup>, Y. Z. Sun<sup>1</sup>, Z. Q. Sun<sup>1,66</sup>, Z. T. Sun<sup>51</sup>, C. J. Tang<sup>55</sup>, G. Y. Tang<sup>1</sup>, J. Tang<sup>61</sup>, J. J. Tang<sup>74,60</sup>, L. F. Tang<sup>40</sup>, Y. A. Tang<sup>79</sup>, L. Y. Tao<sup>75</sup>, M. Tat<sup>72</sup>, J. X. Teng<sup>74,60</sup>, J. Y. Tian<sup>74,60</sup>, W. H. Tian<sup>61</sup>, Y. Tian<sup>32</sup>, Z. F. Tian<sup>79</sup>, I. Uman<sup>64B</sup>, B. Wang<sup>61</sup>, B. Wang<sup>1</sup>, Bo Wang<sup>74,60</sup>, C. Wang<sup>39,k,l</sup>, C. Wang<sup>20</sup>, Cong Wang<sup>23</sup>, D. Y. Wang<sup>47,h</sup>, H. J. Wang<sup>39,k,l</sup>, J. J. Wang<sup>79</sup>, K. Wang<sup>1,60</sup>, L. L. Wang<sup>1</sup>, L. W. Wang<sup>35</sup>, M. Wang<sup>74,60</sup>, M. Wang<sup>51</sup>, N. Y. Wang<sup>66</sup>, Shun Wang<sup>59</sup>, T. Wang<sup>12,g</sup>, T. J. Wang<sup>44</sup>, W. Wang<sup>61</sup>, W. Wang<sup>75</sup>, W. P. Wang<sup>36</sup>, X. Wang<sup>47,h</sup>, X. F. Wang<sup>39,k,l</sup>, X. J. Wang<sup>40</sup>, X. L. Wang<sup>12,g</sup>, X. N. Wang<sup>1,66</sup>, Y. Wang<sup>63</sup>, Y. D. Wang<sup>46</sup>, Y. F. Wang<sup>1,8,66</sup>, Y. H. Wang<sup>39,k,l</sup>, Y. J. Wang<sup>74,60</sup>, Y. L. Wang<sup>20</sup>, Y. N. Wang<sup>79</sup>, Y. Q. Wang<sup>1</sup>, Yaqian Wang<sup>18</sup>, Yi Wang<sup>63</sup>, Yuan Wang<sup>18,32</sup>, Z. Wang<sup>1,60</sup>, Z. L. Wang<sup>2</sup>, Z. L. Wang<sup>75</sup>, Z. Q. Wang<sup>12,g</sup>, Z. Y. Wang<sup>1,66</sup>, D. H. Wei<sup>14</sup>, H. R. Wei<sup>44</sup>, F. Weidner<sup>71</sup>, S. P. Wen<sup>1</sup>, Y. R. Wen<sup>40</sup>, U. Wiedner<sup>3</sup>, G. Wilkinson<sup>72</sup>, M. Wolke<sup>78</sup>, C. Wu<sup>40</sup>, J. F. Wu<sup>1,8</sup>, L. H. Wu<sup>1</sup>, L. J. Wu<sup>20</sup>, L. J. Wu<sup>1,66</sup>, Lianjie Wu<sup>20</sup>, S. G. Wu<sup>1,66</sup>, S. M. Wu<sup>66</sup>, X. Wu<sup>12,g</sup>, X. H. Wu<sup>35</sup>, Y. J. Wu<sup>32</sup>, Z. Wu<sup>1,60</sup>, L. Xia<sup>74,60</sup>, X. M. Xian<sup>40</sup>, B. H. Xiang<sup>1,66</sup>, D. Xiao<sup>39,k,l</sup>, G. Y. Xiao<sup>43</sup>, H. Xiao<sup>75</sup>, Y. L. Xiao<sup>12,g</sup>, Z. J. Xiao<sup>42</sup>, C. Xie<sup>43</sup>, K. J. Xie<sup>1,66</sup>, X. H. Xie<sup>47,h</sup>, Y. Xie<sup>51</sup>, Y. G. Xie<sup>1,60</sup>, Y. H. Xie<sup>6</sup>, Z. P. Xie<sup>74,60</sup>, T. Y. Xing<sup>1,66</sup>, C. F. Xu<sup>1,66</sup>, C. J. Xu<sup>61</sup>, G. F. Xu<sup>1</sup>, H. Y. Xu<sup>69,2</sup>, H. Y. Xu<sup>2</sup>, M. Xu<sup>74,60</sup>, Q. J. Xu<sup>17</sup>, Q. N. Xu<sup>31</sup>, T. D. Xu<sup>75</sup>, W. Xu<sup>1</sup>, W. L. Xu<sup>69</sup>, X. P. Xu<sup>56</sup>, Y. Xu<sup>12,g</sup>, Y. Xu<sup>41</sup>, Y. C. Xu<sup>80</sup>, Z. S. Xu<sup>66</sup>, F. Yan<sup>12,g</sup>, H. Y. Yan<sup>40</sup>, L. Yan<sup>12,g</sup>, W. B. Yan<sup>74,60</sup>,

W. C. Yan<sup>83</sup>, W. H. Yan<sup>6</sup>, W. P. Yan<sup>20</sup>, X. Q. Yan<sup>1,66</sup>, H. J. Yang<sup>52,f</sup>, H. L. Yang<sup>35</sup>, H. X. Yang<sup>1</sup>, J. H. Yang<sup>43</sup>, R. J. Yang<sup>20</sup>, T. Yang<sup>1</sup>, Y. Yang<sup>12,g</sup>, Y. F. Yang<sup>44</sup>, Y. H. Yang<sup>43</sup>, Y. Q. Yang<sup>9</sup>, Y. X. Yang<sup>1,66</sup>, Y. Z. Yang<sup>20</sup>, M. Ye<sup>1,60</sup>, M. H. Ye<sup>8,a</sup>, Z. J. Ye<sup>57,j</sup>, Junhao Yin<sup>44</sup>, Z. Y. You<sup>61</sup>, B. X. Yu<sup>1,60,66</sup>, C. X. Yu<sup>44</sup>, G. Yu<sup>13</sup>, J. S. Yu<sup>26,i</sup>, L. Q. Yu<sup>12,g</sup>, M. C. Yu<sup>41</sup>, T. Yu<sup>75</sup>, X. D. Yu<sup>47,h</sup>, Y. C. Yu<sup>83</sup>, C. Z. Yuan<sup>1,66</sup>, H. Yuan<sup>1,66</sup>, J. Yuan<sup>35</sup>, J. Yuan<sup>46</sup>, L. Yuan<sup>2</sup>, S. C. Yuan<sup>1,66</sup>, S. H. Yuan<sup>75</sup>, X. Q. Yuan<sup>1</sup>, Y. Yuan<sup>1,66</sup>, Z. Y. Yuan<sup>61</sup>, C. X. Yue<sup>40</sup>, Ying Yue<sup>20</sup>, A. A. Zafar<sup>76</sup>, S. H. Zeng<sup>65</sup>, X. Zeng<sup>12,g</sup>, Y. Zeng<sup>26,i</sup>, Y. J. Zeng<sup>61</sup>, Y. J. Zeng<sup>1,66</sup>, X. Y. Zhai<sup>35</sup>, Y. H. Zhan<sup>61</sup>, Zhang<sup>72</sup>, A. Q. Zhang<sup>1,66</sup>, B. L. Zhang<sup>1,66</sup>, B. X. Zhang<sup>1</sup>, D. H. Zhang<sup>44</sup>, G. Y. Zhang<sup>1,66</sup>, G. Y. Zhang<sup>20</sup>, H. Zhang<sup>74,60</sup>, H. Zhang<sup>83</sup>, H. C. Zhang<sup>1,60,66</sup>, H. H. Zhang<sup>61</sup>, H. Q. Zhang<sup>1,60,66</sup>, H. R. Zhang<sup>74,60</sup>, H. Y. Zhang<sup>1,60</sup>, J. Zhang<sup>83</sup>, J. Zhang<sup>61</sup>, J. J. Zhang<sup>53</sup>, J. L. Zhang<sup>21</sup>, J. Q. Zhang<sup>42</sup>, J. S. Zhang<sup>12,g</sup>, J. W. Zhang<sup>1,60,66</sup>, J. X. Zhang<sup>39,k,l</sup>, J. Y. Zhang<sup>1</sup>, J. Z. Zhang<sup>1,66</sup>, Jianyu Zhang<sup>66</sup>, L. M. Zhang<sup>63</sup>, Lei Zhang<sup>43</sup>, N. Zhang<sup>83</sup>, P. Zhang<sup>1,8</sup>, Q. Zhang<sup>20</sup>, Q. Y. Zhang<sup>35</sup>, R. Y. Zhang<sup>39,k,l</sup>, S. H. Zhang<sup>1,66</sup>, Shulei Zhang<sup>26,i</sup>, X. M. Zhang<sup>1</sup>, X. Y. Zhang<sup>41</sup>, X. Y. Zhang<sup>51</sup>, Y. Zhang<sup>1</sup>, Y. Zhang<sup>75</sup>, Y. T. Zhang<sup>83</sup>, Y. H. Zhang<sup>1,60</sup>, Y. M. Zhang<sup>40</sup>, Y. P. Zhang<sup>74,60</sup>, Z. D. Zhang<sup>1</sup>, Z. H. Zhang<sup>1</sup>, Z. L. Zhang<sup>56</sup>, Z. L. Zhang<sup>35</sup>, Z. X. Zhang<sup>20</sup>, Z. Y. Zhang<sup>44</sup>, Z. Y. Zhang<sup>79</sup>, Z. Z. Zhang<sup>46</sup>, Zh. Zh. Zhang<sup>20</sup>, G. Zhao<sup>1</sup>, J. Y. Zhao<sup>1,66</sup>, J. Z. Zhao<sup>1,60</sup>, L. Zhao<sup>1</sup>, L. Zhao<sup>74,60</sup>, M. G. Zhao<sup>44</sup>, N. Zhao<sup>81</sup>, R. P. Zhao<sup>66</sup>, S. J. Zhao<sup>83</sup>, Y. B. Zhao<sup>1,60</sup>, Y. L. Zhao<sup>56</sup>, Y. X. Zhao<sup>32,66</sup>, Z. G. Zhao<sup>74,60</sup>, A. Zhemchugov<sup>37,b</sup>, B. Zheng<sup>75</sup>, B. M. Zheng<sup>35</sup>, J. P. Zheng<sup>1,60</sup>, W. J. Zheng<sup>1,66</sup>, X. R. Zheng<sup>20</sup>, Y. H. Zheng<sup>66,p</sup>, B. Zhong<sup>42</sup>, C. Zhong<sup>20</sup>, H. Zhou<sup>36,51,o</sup>, J. Q. Zhou<sup>35</sup>, J. Y. Zhou<sup>35</sup>, S. Zhou<sup>6</sup>, X. Zhou<sup>79</sup>, X. K. Zhou<sup>6</sup>, X. R. Zhou<sup>74,60</sup>, X. Y. Zhou<sup>40</sup>, Y. X. Zhou<sup>80</sup>, Y. Z. Zhou<sup>12,g</sup>, A. N. Zhu<sup>66</sup>, J. Zhu<sup>44</sup>, K. Zhu<sup>1</sup>, K. J. Zhu<sup>1,60,66</sup>, K. S. Zhu<sup>12,g</sup>, L. Zhu<sup>35</sup>, L. X. Zhu<sup>66</sup>, S. H. Zhu<sup>73</sup>, T. J. Zhu<sup>12,g</sup>, W. D. Zhu<sup>12,g</sup>, W. D. Zhu<sup>42</sup>, W. J. Zhu<sup>1</sup>, W. Z. Zhu<sup>20</sup>, Y. C. Zhu<sup>74,60</sup>, Z. A. Zhu<sup>1,66</sup>, X. Y. Zhuang<sup>44</sup>, J. H. Zou<sup>1</sup>, J. Zu<sup>74,60</sup>

---

<sup>1</sup> Institute of High Energy Physics, Beijing 100049, People's Republic of China

<sup>2</sup> Beihang University, Beijing 100191, People's Republic of China

<sup>3</sup> Bochum Ruhr-University, D-44780 Bochum, Germany

<sup>4</sup> Budker Institute of Nuclear Physics SB RAS (BINP), Novosibirsk 630090, Russia

<sup>5</sup> Carnegie Mellon University, Pittsburgh, Pennsylvania 15213, USA

<sup>6</sup> Central China Normal University, Wuhan 430079, People's Republic of China

<sup>7</sup> Central South University, Changsha 410083, People's Republic of China

<sup>8</sup> China Center of Advanced Science and Technology, Beijing 100190, People's Republic of China

<sup>9</sup> China University of Geosciences, Wuhan 430074, People's Republic of China

<sup>10</sup> Chung-Ang University, Seoul, 06974, Republic of Korea

<sup>11</sup> COMSATS University Islamabad, Lahore Campus, Defence Road, Off Raiwind Road, 54000 Lahore, Pakistan

<sup>12</sup> Fudan University, Shanghai 200433, People's Republic of China

<sup>13</sup> GSI Helmholtzcentre for Heavy Ion Research GmbH, D-64291 Darmstadt, Germany

<sup>14</sup> Guangxi Normal University, Guilin 541004, People's Republic of China

<sup>15</sup> Guangxi University, Nanning 530004, People's Republic of China

<sup>16</sup> Guangxi University of Science and Technology, Liuzhou 545006, People's Republic of China

<sup>17</sup> Hangzhou Normal University, Hangzhou 310036, People's Republic of China

<sup>18</sup> Hebei University, Baoding 071002, People's Republic of China

<sup>19</sup> Helmholtz Institute Mainz, Staudinger Weg 18, D-55099 Mainz, Germany

<sup>20</sup> Henan Normal University, Xinxiang 453007, People's Republic of China

<sup>21</sup> Henan University, Kaifeng 475004, People's Republic of China

<sup>22</sup> Henan University of Science and Technology, Luoyang 471003, People's Republic of China

<sup>23</sup> Henan University of Technology, Zhengzhou 450001, People's Republic of China

<sup>24</sup> Huangshan College, Huangshan 245000, People's Republic of China

<sup>25</sup> Hunan Normal University, Changsha 410081, People's Republic of China

<sup>26</sup> Hunan University, Changsha 410082, People's Republic of China

- <sup>27</sup> Indian Institute of Technology Madras, Chennai 600036, India
- <sup>28</sup> Indiana University, Bloomington, Indiana 47405, USA
- <sup>29</sup> INFN Laboratori Nazionali di Frascati, (A)INFN Laboratori Nazionali di Frascati, I-00044, Frascati, Italy; (B)INFN Sezione di Perugia, I-06100, Perugia, Italy; (C)University of Perugia, I-06100, Perugia, Italy
- <sup>30</sup> INFN Sezione di Ferrara, (A)INFN Sezione di Ferrara, I-44122, Ferrara, Italy; (B)University of Ferrara, I-44122, Ferrara, Italy
- <sup>31</sup> Inner Mongolia University, Hohhot 010021, People's Republic of China
- <sup>32</sup> Institute of Modern Physics, Lanzhou 730000, People's Republic of China
- <sup>33</sup> Institute of Physics and Technology, Mongolian Academy of Sciences, Peace Avenue 54B, Ulaanbaatar 13330, Mongolia
- <sup>34</sup> Instituto de Alta Investigación, Universidad de Tarapacá, Casilla 7D, Arica 1000000, Chile
- <sup>35</sup> Jilin University, Changchun 130012, People's Republic of China
- <sup>36</sup> Johannes Gutenberg University of Mainz, Johann-Joachim-Becher-Weg 45, D-55099 Mainz, Germany
- <sup>37</sup> Joint Institute for Nuclear Research, 141980 Dubna, Moscow region, Russia
- <sup>38</sup> Justus-Liebig-Universität Giessen, II. Physikalisches Institut, Heinrich-Buff-Ring 16, D-35392 Giessen, Germany
- <sup>39</sup> Lanzhou University, Lanzhou 730000, People's Republic of China
- <sup>40</sup> Liaoning Normal University, Dalian 116029, People's Republic of China
- <sup>41</sup> Liaoning University, Shenyang 110036, People's Republic of China
- <sup>42</sup> Nanjing Normal University, Nanjing 210023, People's Republic of China
- <sup>43</sup> Nanjing University, Nanjing 210093, People's Republic of China
- <sup>44</sup> Nankai University, Tianjin 300071, People's Republic of China
- <sup>45</sup> National Centre for Nuclear Research, Warsaw 02-093, Poland
- <sup>46</sup> North China Electric Power University, Beijing 102206, People's Republic of China
- <sup>47</sup> Peking University, Beijing 100871, People's Republic of China
- <sup>48</sup> Qufu Normal University, Qufu 273165, People's Republic of China
- <sup>49</sup> Renmin University of China, Beijing 100872, People's Republic of China
- <sup>50</sup> Shandong Normal University, Jinan 250014, People's Republic of China
- <sup>51</sup> Shandong University, Jinan 250100, People's Republic of China
- <sup>52</sup> Shanghai Jiao Tong University, Shanghai 200240, People's Republic of China
- <sup>53</sup> Shanxi Normal University, Linfen 041004, People's Republic of China
- <sup>54</sup> Shanxi University, Taiyuan 030006, People's Republic of China
- <sup>55</sup> Sichuan University, Chengdu 610064, People's Republic of China
- <sup>56</sup> Soochow University, Suzhou 215006, People's Republic of China
- <sup>57</sup> South China Normal University, Guangzhou 510006, People's Republic of China
- <sup>58</sup> Southeast University, Nanjing 211100, People's Republic of China
- <sup>59</sup> Southwest University of Science and Technology, Mianyang 621010, People's Republic of China
- <sup>60</sup> State Key Laboratory of Particle Detection and Electronics, Beijing 100049, Hefei 230026, People's Republic of China
- <sup>61</sup> Sun Yat-Sen University, Guangzhou 510275, People's Republic of China
- <sup>62</sup> Suranaree University of Technology, University Avenue 111, Nakhon Ratchasima 30000, Thailand
- <sup>63</sup> Tsinghua University, Beijing 100084, People's Republic of China
- <sup>64</sup> Turkish Accelerator Center Particle Factory Group, (A)Istinye University, 34010, Istanbul, Turkey; (B)Near East University, Nicosia, North Cyprus, 99138, Mersin 10, Turkey
- <sup>65</sup> University of Bristol, H H Wills Physics Laboratory, Tyndall Avenue, Bristol, BS8 1TL, UK
- <sup>66</sup> University of Chinese Academy of Sciences, Beijing 100049, People's Republic of China
- <sup>67</sup> University of Groningen, NL-9747 AA Groningen, The Netherlands
- <sup>68</sup> University of Hawaii, Honolulu, Hawaii 96822, USA
- <sup>69</sup> University of Jinan, Jinan 250022, People's Republic of China
- <sup>70</sup> University of Manchester, Oxford Road, Manchester, M13 9PL, United Kingdom
- <sup>71</sup> University of Muenster, Wilhelm-Klemm-Strasse 9, 48149 Muenster, Germany
- <sup>72</sup> University of Oxford, Keble Road, Oxford OX13RH, United Kingdom
- <sup>73</sup> University of Science and Technology Liaoning, Anshan 114051, People's Republic of China
- <sup>74</sup> University of Science and Technology of China, Hefei 230026, People's Republic of China
- <sup>75</sup> University of South China, Hengyang 421001, People's Republic of China
- <sup>76</sup> University of the Punjab, Lahore-54590, Pakistan
- <sup>77</sup> University of Turin and INFN, (A)University of Turin, I-10125, Turin, Italy; (B)University of Eastern Piedmont, I-15121, Alessandria, Italy; (C)INFN, I-10125, Turin, Italy
- <sup>78</sup> Uppsala University, Box 516, SE-75120 Uppsala, Sweden
- <sup>79</sup> Wuhan University, Wuhan 430072, People's Republic of China
- <sup>80</sup> Yantai University, Yantai 264005, People's Republic of China
- <sup>81</sup> Yunnan University, Kunming 650500, People's Republic of China
- <sup>82</sup> Zhejiang University, Hangzhou 310027, People's Republic of China
- <sup>83</sup> Zhengzhou University, Zhengzhou 450001, People's Republic of China
- <sup>a</sup> Deceased
- <sup>b</sup> Also at the Moscow Institute of Physics and Technology, Moscow 141700, Russia
- <sup>c</sup> Also at the Novosibirsk State University, Novosibirsk, 630090, Russia
- <sup>d</sup> Also at the NRC "Kurchatov Institute", PNPI, 188300, Gatchina, Russia
- <sup>e</sup> Also at Goethe University Frankfurt, 60323 Frankfurt am Main, Germany
- <sup>f</sup> Also at Key Laboratory for Particle Physics, Astrophysics and Cosmology, Ministry of Education; Shanghai Key Laboratory for Particle Physics and Cosmology; Institute of Nuclear and Particle Physics, Shanghai 200240, People's Republic of China
- <sup>g</sup> Also at Key Laboratory of Nuclear Physics and Ion-beam Application (MOE) and Institute of Modern Physics, Fudan University,

Shanghai 200443, People's Republic of China

<sup>h</sup> Also at State Key Laboratory of Nuclear Physics and Technology, Peking University, Beijing 100871, People's Republic of China

<sup>i</sup> Also at School of Physics and Electronics, Hunan University, Changsha 410082, China

<sup>j</sup> Also at Guangdong Provincial Key Laboratory of Nuclear Science, Institute of Quantum Matter, South China Normal University, Guangzhou 510006, China

<sup>k</sup> Also at MOE Frontiers Science Center for Rare Isotopes, Lanzhou University, Lanzhou 730000, People's Republic of China

<sup>l</sup> Also at Lanzhou Center for Theoretical Physics, Lanzhou University, Lanzhou 730000, People's Republic of China

<sup>m</sup> Also at the Department of Mathematical Sciences, IBA, Karachi 75270, Pakistan

<sup>n</sup> Also at Ecole Polytechnique Federale de Lausanne (EPFL), CH-1015 Lausanne, Switzerland

<sup>o</sup> Also at Helmholtz Institute Mainz, Staudinger Weg 18, D-55099 Mainz, Germany

<sup>p</sup> Also at Hangzhou Institute for Advanced Study, University of Chinese Academy of Sciences, Hangzhou 310024, China

<sup>q</sup> Currently at: Silesian University in Katowice, Chorzow, 41-500, Poland

## Acknowledgement

The BESIII Collaboration thanks the staff of BEPCII (<https://cstr.cn/31109.02.BEPC>) and the IHEP computing center for their strong support. This work is supported in part by National Key R&D Program of China under Contracts Nos. 2023YFA1606704, 2023YFA1606000; National Natural Science Foundation of China (NSFC) under Contracts Nos. 12375092, 11635010, 11935015, 11935016, 11935018, 12025502, 12035009, 12035013, 12061131003, 12192260, 12192261, 12192262, 12192263, 12192264, 12192265, 12221005, 12225509, 12235017, 12361141819; Beijing Natural Science Foundation of China (BNSF) under Contract No. IS23014; The Chinese Academy of Sciences (CAS) Large-Scale Scientific Facility Program; CAS under Contract No. YSBR-101; 100 Talents Program of CAS; The Institute of Nuclear and Particle Physics (INPAC) and Shanghai Key Laboratory for Particle Physics and Cosmology; ERC under Contract No. 758462; German Research Foundation DFG under Contract No. FOR5327; Istituto Nazionale di Fisica Nucleare, Italy; Knut and Alice Wallenberg Foundation under Contracts Nos. 2021.0174, 2021.0299; Ministry of Development of Turkey under Contract No. DPT2006K-120470; National Research Foundation of Korea under Contract No. NRF-2022R1A2C1092335; National Science and Technology fund of Mongolia; Polish National Science Centre under Contract No. 2024/53/B/ST2/00975; STFC (United Kingdom); Swedish Research Council under Contracts Nos. 2019.04595, 2021.04567; the Olle Engkvist Foundation under Contract No. 200-0605; U. S. Department of Energy under Contract No. DE-FG02-05ER41374.